Gondwana Research xxx (2014) xxx–xxx

Contents lists available at ScienceDirect

Gondwana Research

journal homepage: www.elsevier.com/locate/gr

Zircon ages and Nd–Hf isotopes in UHT granulites of the Ider Complex: A cratonic terrane within the Central Asian Orogenic Belt in NW Mongolia

A. Kröner [a,b,*], V.P. Kovach [c], I.K. Kozakov [c], T. Kirnozova [d], P. Azimov [c], J. Wong [e], H.Y. Geng [e]

[a] Beijing SHRIMP Centre, Institute of Geology, Chinese Academy of Geological Sciences, 26 Baiwanzhuang Road, 100037 Beijing, China
[b] Department of Geosciences, University of Mainz, 55099 Mainz, Germany
[c] Institute of Precambrian Geology and Geochronology, Russian Academy of Sciences, nab. Makarova 2, St. Petersburg, 199034 Russia
[d] Vernadsky Institute of Geochemistry and Analytical Chemistry, Russian Academy of Sciences, ul. Kosygina 19, Moscow, 119991 Russia
[e] Department of Earth Sciences, University of Hong Kong, Pokfulam Road, Hong Kong, China

ARTICLE INFO

Article history:
Received 24 January 2014
Received in revised form 6 March 2014
Accepted 14 March 2014
Available online xxxx

Handling Editor: M. Santosh

Keywords:
Central Asian Orogenic Belt
Granulite
Zircon dating
Nd–Hf isotopes
Tarbagatai microcontinent

ABSTRACT

The Ider Complex of the Tarbagatai Block in northwestern Mongolia is part of a Precambrian microcontinental terrane in the Central Asian Orogen Belt and has experienced a polymetamorphic tectono-metamorphic evolution. We have investigated an enderbitic gneiss, derived from a quartz diorite and a charnockite, derived from a leucogranite, and zircon SHRIMP data reveal late Archaean protolith ages of 2520–2546 Ma for these rocks. Metamorphic overgrowth on these zircons as well as newly-formed metamorphic zircons document a high-temperature metamorphic event (T = 930–950 °C) at about 1855–1860 Ma. Nd whole-rock isotopic systematics show these and other gneisses of the Ider Complex straddling the CHUR-line in a Nd isotope evolution diagram, suggesting both crustal reworking and input of some juvenile material, with Nd model ages ranging between ca. 2.5 and 3.1 Ga. Hf-in-zircon isotopic data provide a similar pattern and also yielded Archaean Hf crustal model ages. The metamorphic zircons seem to have inherited their Hf isotopic composition from the igneous grains, suggesting a complex process of dissolution, transportation, and re-precipitation involving a fluid phase during high-grade metamorphism. The zircon age patterns do not make it possible to unambiguously assign the Tarbagatai Block to any of the cratons bordering the Central Asian Orogenic Belt, since age peaks at ca. 2520–2550 and ca. 1860 Ma are common in the Siberian, North China and Tarim cratons.

1. Introduction

The broad terrane of southern Siberia and Mongolia south of the Siberian craton is part of the Central Asian Orogenic Belt (CAOB). It consists of Neoproterozoic to early Paleozoic island arc and ophiolite complexes as well as fragments of continental massifs that were tectonically juxtaposed during accretionary orogenic events in the Paleozoic (Mossakovsky et al., 1993; Kovach et al., 2004; Kovalenko et al, 2005; Kozakov et al., 2008, 2011; Yarmolyuk et al., 2011; Kröner et al., 2014).

The oldest of these continental massifs consists of crystalline rocks dating back to the Archaean and may be rifted-off fragments of ancient cratons. Single zircon ages as well as whole-rock Sm–Nd and Pb–Pb isotopic data indicate that Archaean to Paleoproterozoic rocks only occur in the Baidarik Block, the Ider Complex of the Tarbagatai Block all in northwestern Mongolia, (Kozakov et al., 2007, 2011), and in the Gargan Block of East Sayan in southern Siberia (Kovach et al., 2004; Anisimova et al., 2009a) (Fig. 1).

The zircon age of tonalitic gneisses in the Gargan Block is 2727 ± 6 Ma (Anisimova et al., 2009a) and the age of high-temperature metamorphism is 2664 ± 15 Ma (Kovach et al., 2004), but the P–T conditions of metamorphism are not well defined. In contrast, the oldest zircon age of a granite-gneiss of the Tarbagatai Block is 2219 ± 25 Ma (Kozakov et al., 2011).

The most detailed geochronological information is available for the Baidarik Block where the oldest zircon age is 2646 ± 45 Ma for tonalitic gneisses of the Baidrag Complex (Mitrofanov et al., 1981). Detailed SHRIMP dating has shown that the oldest components are $^{207}Pb/^{206}Pb$ core ages at around 2.8 Ga, and the main group of zircons yielded $^{207}Pb/^{206}Pb$ ages of 2.50–2.65 Ga, including grains as typically found in granulite-facies rocks (Kozakov et al., 2007). Mapping and zircon dating of granitoid gneisses have also documented a major tectono-metamorphic event at 1854–1825 Ma and an earlier granulite-facies metamorphism in the Bumbuger Complex of the Baidarik Block between 2364 and 2308 Ma (Kozakov et al., 2007; Demoux et al., 2009).

Thus, only two localities of early Precambrian basement are currently known in the northern CAOB. Here we present new age data and Hf-in-zircon isotopic compositions for granulite-facies rocks in the early Precambrian Ider Complex of the Tarbagatai Block and discuss their sources and tectonic setting.

* Corresponding author.

http://dx.doi.org/10.1016/j.gr.2014.03.005
1342-937X/

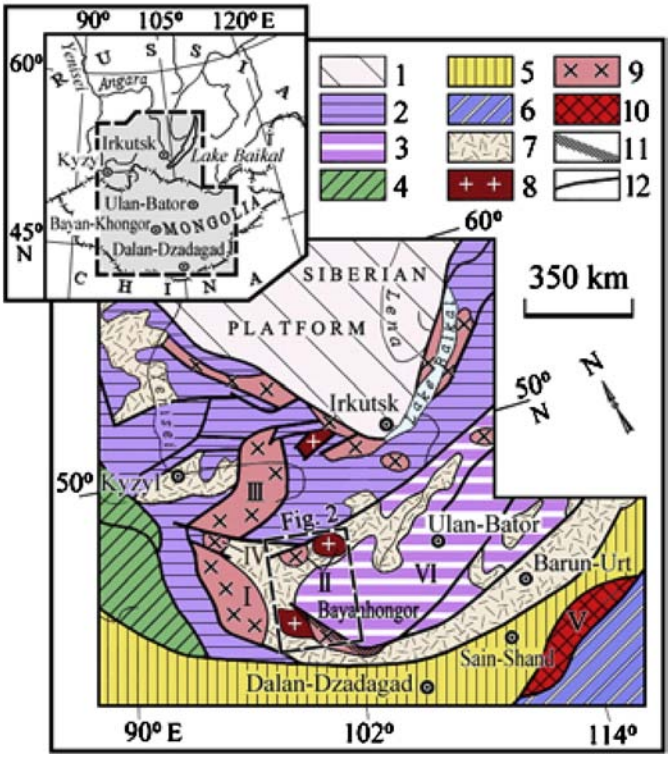

Fig. 1. Location of crystalline complexes in the eastern segment of the Central Asian Orogenic Belt (from Kozakov et al., 2011). (1) Ancient platforms; (2) Early Paleozoic assemblages; (3) undivided Precambrian blocks of the Hangay Group, overlain by Paleozoic sequences; (4) Mid-Paleozoic assemblages; (5) late Paleozoic assemblages; (6) Mid-Mesozoic assemblages; (7) Phanerozoic volcano-plutonic belts; (8–10) fragments of continental massifs: (8) with early Precambrian (?) basement; (9) with Neoproterozoic basement; (10) with Mesoproterozoic basement; (11) Bayankhongor ophiolite belt; (12) main tectonic boundaries. Roman numbers: (I) Dzabkhan microcontinent, (II) Tarbagatai group of blocks, (III) Tuva–Mongolian microcontinens, (IV) Songino block, (V) South Gobi block, and (VI) Hangay block overlain by Paleozoic–Mesozoic sediments. Inset shows location of Fig. 1 in Central Asia. Circled numbers: (1) Tuva–Mongolia and (2) Dzabkhan microcontinents; (3) Tarbagatai Block; and (4) Songino Block.

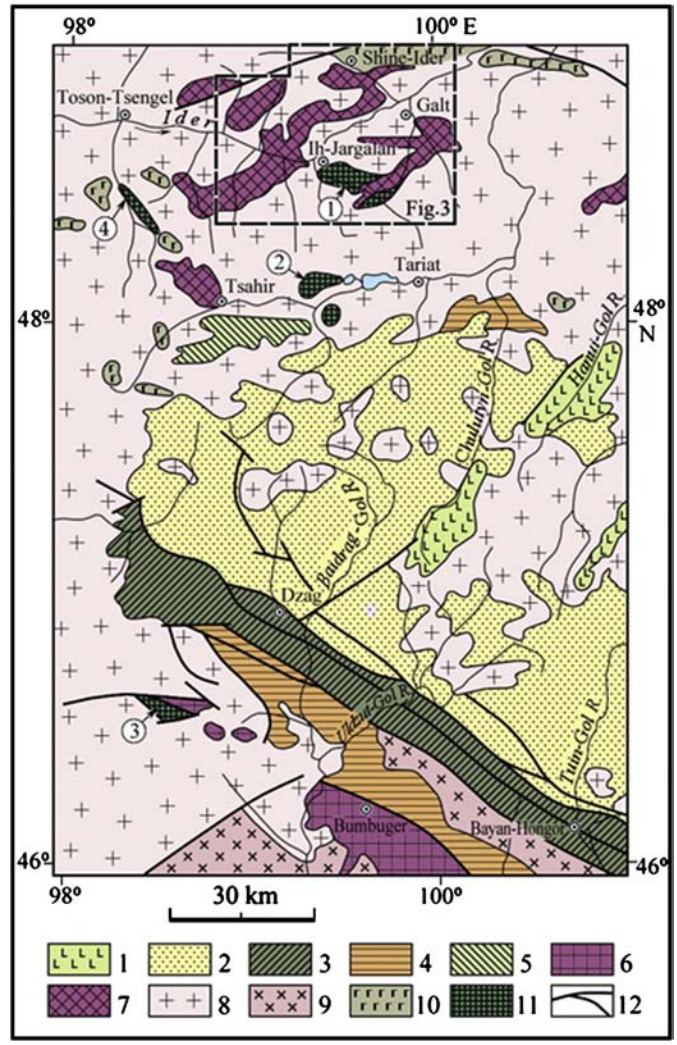

Fig. 2. Location of early Precambrian complexes in Central and NW Mongolia (from Kozakov et al, 2011). (1) Cenozoic basalts; (2) Devonian and Carboniferous sediments (Hangay Group) of the Hangay synclinorium; (3) Bayankhongor ophiolite belt; (4) Neoproterozoic shelf sediments of the Dzabkhan microcontinent (Uldzitgol Complex); (5) undifferentiated Neoproterozoic volcano-plutonic rocks, (6) early Precambrian crystalline complexes of the Baidarik Block of the Dzabkhan microcontinent; (7) crystalline complexes of the Tarbagatai Block; (8) Permian volcanic rocks and plutonic units of the Hangay Batholith; (9) undifferentiated early Paleozoic granitoids; (10) undifferentiated late Neoproterozoic–early Paleozoic gabbroic intrusives; (11) Paleoproterozoic anorthosites; (12) main tectonic boundaries and faults. Circled numbers denote anorthosite plutons: (1) Hunzhilingol (1784 ± 10 Ma), (2) Mustulin, (3) Olonkhuduk, and (4) Hodzhulingol. Inset shows location of Fig. 3.

2. Geology of the Tarbagatai Block

Crystalline rocks of the Tarbagatai Block were first considered to be the part of the Dzabkhan microcontinent (Mossakovsky et al., 1993) and were later defined as the Tarbagatai cratonic terrane (Badarch et al, 2002). However, they constitute several large but separate blocks enclosed in the Permian Khangay batholith and are structurally isolated from the Dzabhan microcontinent and the Baidarik block (Fig. 2). Amongst the Tarbagatai crystalline rocks an early Precambrian and a Neoproterozoic domain were recognized and named the Ider and Jargalant Complexes, respectively (Fig. 3). Originally, high-temperature regional metamorphism was the criterion for considering the Ider Complex to be early Precambrian in age.

The Ider Complex consists of strongly migmatized biotite and hornblende orthogneisses with rare inclusions of amphibolite and granite-gneiss bodies; sillimanite-bearing paragneisses occur in subordinate quantities. An early high-grade metamorphism produced granulite-facies assemblages as indicated by inclusions of two-pyroxene-bearing gneiss, enderbite and charnockite (Table 1). The central parts of such inclusions remained unaffected by amphibolite facies retrogressive (regional) metamorphism, and relict parageneses are: *clinopyroxene ± brown hornblende + plagioclase ± quartz* and *clinopyroxene + plagioclase + orthoclase + quartz*. Charnockite formation is documented by the paragenesis *orthopyroxene + plagioclase + orthoclase + quartz*, and enderbites contain the paragenesis *orthopyroxene + plagioclase with antiperthite + quartz + biotite*. Pyroxene is replaced by green hornblende in the marginal parts of such granulite inclusions. In general, as a result of amphibolite-facies retrograde regional metamorphism, many pyroxene-bearing gneisses were downgraded into amphibole gneisses or schists, and dark colored minerals such as biotite and/or green hornblende are present in most migmatites.

Retrograde metamorphism of the granulite-facies assemblages was accompanied by widespread migmatization, culminating in the injection of numerous granitoid veins with a width of a few tens of centimeters to 1.5–2 m. These granitoids cut across the migmatite layering, and in areas of high strain they are folded together with the migmatites and these domains become well foliated, gneissose granite. The zircon age of one of these granite-gneisses is 2219 ± 25 Ma (Kozakov et al., 2011). Later, more massive, granitoids also occur in the migmatites and make up irregularly-shaped bodies with indistinct contacts over an area of more than several hundred square meters. The established zircon age range for these granitoids is about 1870–1860 Ma (Kozakov et al, 2011).

Generation of the main foliation and structures of the Ider Complex and amphibolite-facies regional metamorphism occurred prior to

Please cite this article as: Kröner, A., et al., Zircon ages and Nd–Hf isotopes in UHT granulites of the Ider Complex: A cratonic terrane within the Central Asian Orogenic Belt in..., Gondwana Research (2014), http://dx.doi.org/10.1016/j.gr.2014.03.005

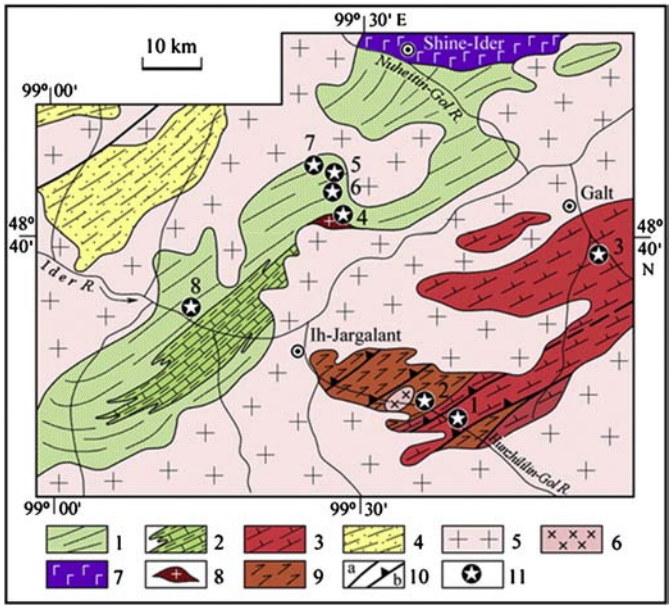

Fig. 3. Simplified geological map of the crystalline complexes in the Tarbagatai Block (from Kozakov et al., 2011). (1–2) *Neoproterozoic Jargalant Complex*: (1) biotite gneiss and (2) interbedded marble, biotite-, and biotite–amphibole gneiss; (3) *Early Precambrian Ider Complex* (strongly migmatized gneisses with relicts of pyroxene-bearing granulites and amphibolites); (4) undifferentiated Precambrian gneiss–migmatite terrane; (5–9) intrusive rocks: (5) granitoids of the Permian Hangay Batholith; (6) Middle Paleozoic granites; (7) Edicaran–early Cambrian gabbroic bodies, (8) Neoproterozoic porphyroblastic granites; (9) gabbro-anorthosite complex of the Hunzhilingol pluton; and (10) shear zones and faults, (a) subvertical, (b) gentle; (11) sampling localities: *Ider Complex*: (1) granite-gneiss (2219 ± 25 Ma), (2) anorthosite of Hunzhilingol pluton (1784 ± 10 Ma), and (3) location of granulite samples (2550 and 1850 Ma). *Jargalant Complex*: (4) granite-gneiss (815 ± 8 Ma); (5) granite-gneiss (809 ± 4 Ma), and granite (797 ± 3 Ma), (6) granite (793 ± 4 Ma); (7) diorite (437 ± 7 Ma), and (8) diorite (421 ± 1 Ma).

the intrusion of anorthosite bodies dated by isotope-dilution TIMS at 1784 ± 10 Ma (Anisimova et al., 2009b). No further deformation and metamorphism occurred after this time. Thus, from the end of the late Paleoproterozoic the crystalline rocks of the Ider Complex were part of a rigid, stable cratonic block and were not affected by deformation and metamorphic events that occurred in the enclosing Neoproterozoic to early Paleozoic rocks during amalgamation of the Central Asian Orogenic Belt. We therefore emphasize that Neoproterozoic regional metamorphism (~800 Ma) and structures as found in the Jargalant Complex (Fig. 3) (Kozakov et al., 2011) did not affect the older Ider Complex.

We have previously attempted to date samples of this complex using the multigrain zircon TIMS method, and our results are summarized below. Because of the discordance of most analyses and the ambiguity of these data in interpreting the geological history of the granulites, we have subsequently used a SHRIMP instrument in combination with cathodoluminescence imagery to understand the complexity of the zircons in these rocks. We have also combined the SHRIMP ages with Hf-in-zircon isotopic analyses in order to unravel the evolution of the dated granulites. Our samples are a charnockite (sample 7011) and enderbite (sample 7340) of the Ider Complex, and their locations are shown in Fig. 3.

3. Field relations and metamorphic conditions of granulite sample 7340

Samples 7340 and 7011 are from the same outcrop of migmatized biotite gneiss and green hornblende gneiss of the Ider Complex which contain rare relicts of granulite-facies rocks such as clinopyroxene and orthopyroxene gneisses, enderbite, and charnockite in amphibolite-facies gneiss and migmatite.

Table 1
Major and trace element composition of gneisses from the Ider Complex[a].

No.	1	2	3	4	5	6	7
Sample no.	6657	6658	7340	7011	6151	6152	6153
SiO_2	64.30	58.40	62.07	73.68	69.80	70.00	70.17
TiO_2	0.90	0.77	0.59	0.05	0.36	0.37	0.19
Al_2O_3	15.00	18.10	16.22	14.70	14.90	15.10	16.50
$Fe_2O_3^t$	5.43	6.38	5.94	0.61	2.67	3.86	2.04
MnO	0.08	0.10	0.09	0.01	0.03	0.04	0.03
MgO	2.18	3.41	3.37	0.27	1.01	0.65	0.53
CaO	4.65	5.60	5.59	1.99	2.57	3.06	2.99
Na_2O	4.29	4.31	4.27	2.88	4.13	4.29	4.94
K_2O	2.27	1.98	1.22	5.11	3.26	1.63	1.69
P_2O_5	0.14	0.31	0.15	0.02	0.14	0.10	0.07
LOI	0.38	0.59	0.47	0.41	0.85	0.61	nd
Total	99.62	99.95	99.98	99.72	99.72	99.71	99.14
$Na_2O + K_2O$	6.56	6.29	5.49	7.99	7.39	5.92	6.63
Na_2O/K_2O	1.89	2.18	3.49	0.56	1.27	2.63	2.93
A/CNK	0.83	0.93	0.88	1.06	0.99	1.05	1.07
Sc	18	10	nd	nd	2.9	2.8	1.5
V	103	108	103	7.1	41	45	12
Cr	43	36	96	6.95	18	23	8.1
Co	17	17	20	2.0	6.7	7.2	2.6
Ni	20	19	54	13	12	13	6.4
Ga	16	20	20	11	20	20	18
Rb	26	37	21	104	62	35	29
Sr	307	608	456	424	726	391	460
Y	21	14	14	0.43	5.7	4.5	2.2
Zr	236	193	94	34	212	226	38
Nb	11	7.1	4.1	0.25	4.8	7.4	1.9
Ba	748	577	442	2450	1680	704	556
La	24	30	16	5.9	58	48	17.4
Ce	53	58	33	9.0	108	85	33
Pr	6.8	7.2	4.5	0.82	9.8	7.7	3.2
Nd	28	29	18.0	2.5	32	23	10.5
Sm	5.5	4.7	3.7	0.22	3.9	3.1	1.46
Eu	1.22	1.63	1.12	0.82	1.31	0.92	0.55
Gd	5.1	4.0	3.5	0.23	2.9	2.0	1.08
Tb	0.74	0.47	0.46	0.016	0.29	0.21	0.110
Dy	3.7	2.6	2.5	0.046	1.09	0.81	0.46
Ho	0.79	0.43	0.54	0.010	0.18	0.140	0.075
Er	2.4	1.20	1.44	0.026	0.55	0.43	0.20
Tm	0.43	0.140	0.24	0.010	0.062	0.07	0.029
Yb	2.1	1.12	1.38	0.036	0.37	0.40	0.19
Lu	0.26	0.21	0.20	0.007	0.054	0.07	0.033
Hf	6.4	4.3	2.3	1.30	5.0	6.0	1.0
Ta	0.59	0.24	0.11	0.05	0.11	0.31	0.030
Th	1.1	0.37	0.68	1.2	16	16	1.9
U	0.29	0.12	0.18	0.13	0.27	0.37	0.10
La_N/Yb_N	8.2	17.8	7.9	110	106	80.6	60.7
La_N/Sm_N	2.8	4.0	2.7	16.8	9.3	9.9	7.5
Gd_N/Yb_N	2.2	2.8	2.1	5.2	6.2	4.1	4.5
Eu/Eu[a]	0.74	1.12	0.93	11.0	1.14	1.06	1.29
Sr/Y	15	45	32	986	127	87	210

[a] Notes. Samples 1–3 — enderbite, 4 — charnockite, 5–6 — migmatitized Bt gneiss, 7 — Bt granite-gneiss. nd — not determined. A / CNK = Al_2O_3 / ($CaO + Na_2O + K_2O$) (mol.%).

Enderbite sample 7340 represents one of these relicts and was collected from a small granulite-facies inclusion with gradational contact within an amphibolite-facies gneiss. Granulite-facies metamorphic mineral assemblages are found in the central parts of these bodies, whereas in the marginal parts orthopyroxene is replaced by hornblende. Charnockite sample 7011 was collected from a thin (25–30 cm) layered body with a visible length of about 3 m and is concordant with the amphibolite-facies regional foliation (defined by green hornblende) in the enclosing rocks.

Enderbite sample 7340 mainly consists of plagioclase, quartz and orthopyroxene but also contains small biotite flakes and orthoclase rims around biotite and orthopyroxene (Fig. 4). Plagioclase contains orthoclase inclusions (antiperthite), and some biotite flakes are found as ingrowths in orthopyroxene.

The temperature of granulite-facies metamorphism was established from the exchange (Fe/Mg) reaction between orthopyroxene and

Please cite this article as: Kröner, A., et al., Zircon ages and Nd–Hf isotopes in UHT granulites of the Ider Complex: A cratonic terrane within the Central Asian Orogenic Belt in..., Gondwana Research (2014), http://dx.doi.org/10.1016/j.gr.2014.03.005

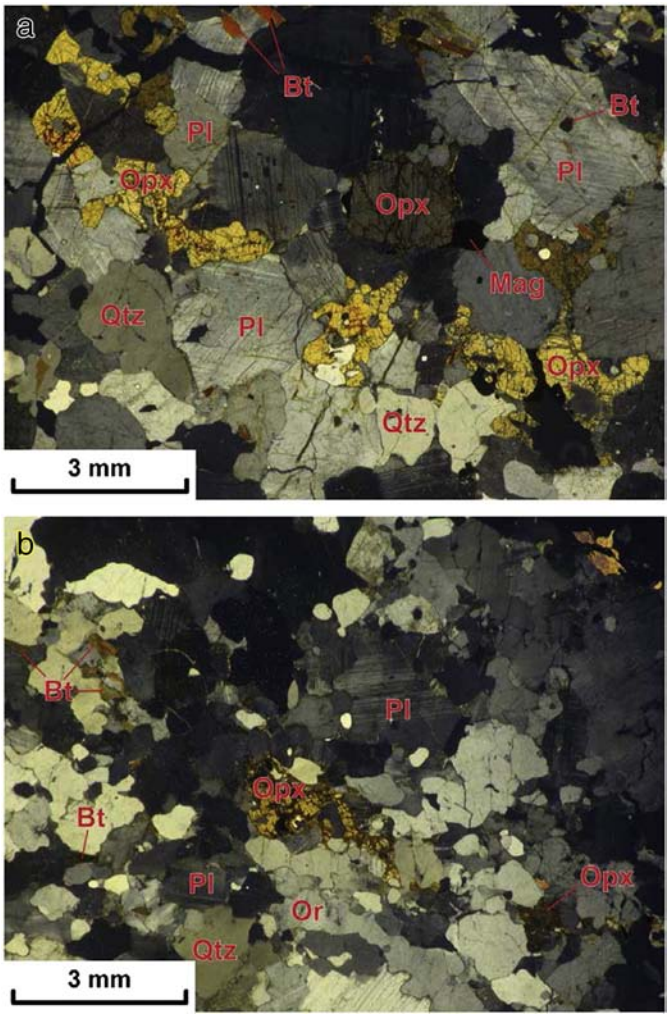

Fig. 4. Texture of biotite–othopyroxene gneiss (BSE image of sample 7340).

biotite (Table 2). Calculations used the TWQ program (Berman, 1991) together with the thermodynamic database BA96a (Aranovich and Berman, 1996; Berman and Aranovich, 1996). Calculation of metamorphic pressure was not possible because of the low alumina content in orthopyroxene (0.5–0.8 wt.% Al_2O_3) and biotite (13.7–14.7 wt.% Al_2O_3), and the lack of garnet in the rock.

The Fe–Mg cation exchange equilibria temperatures calculated for biotite in the rock matrix are 860–950 °C. The highest temperatures (930–950 °C) were determined for biotite flakes in direct contact with orthopyroxene. Temperatures for biotite grains penetrating and replacing orthopyroxene are lower (800–850 °C). This confirms the secondary development of such biotite that formed as a result of decharnockitization (retrogression). The biotite–orthopyroxene exchange reaction in P–T space is close to vertical, hence, the estimated temperature values do not depend on the metamorphic pressure.

The metamorphic peak temperature (>900 °C) is in agreement with the development of antiperthite in plagioclase. Therefore, granulite-facies metamorphism in the Ider Complex can be attributed to an ultrahigh-temperature (UHT) event.

Charnockite sample 7011 with the paragenesis *orthopyroxene + plagioclase + orthoclase + quartz* is preserved in the central part of a layered body. Orthopyroxene disappears in the marginal parts and twinned microcline appears instead of orthoclase. This shows that the granulite-facies rocks (charnockite, enderbite, pyroxene gneiss) were reworked during retrograde amphibolite-facies regional metamorphism.

4. Geochemical characteristic of high-grade rocks in the Ider Complex

Granulites of Ider Complex can be subdivided into two groups according to their composition and chemical features. The first group (samples 6657, 6658 and 7340 in Table 1) correspond to metaluminous quartz diorite and granodiorite with $Na_2O/K_2O = 1.9–3.5$. They are characterized by fractionated trace-elements distribution patterns with negative anomalies in Th, U, Nb–Ta, P and Ti (Fig. 5a), low Sr/Y ratios (15–45), moderately fractionated REE patterns ($La_N/Yb_N = 7.9–17.8$) with gentle slopes of HREE ($Gd_N/Yb_N = 2.1–2.8$), and weak negative and positive Eu anomalies ($Eu/Eu^* = 0.74–1.12$) (Fig. 5b). The geochemical data are compatible with the interpretation that the enderbite protoliths may have formed by partial melting of basaltic source in an island arc or active continental margin setting at a pressure of ~3–7 kbar with *Pl + Cpx + Opx* in the residue.

In contrast to the enderbites, charnockite sample 7011 is characterized by high silica and chemically corresponds to leucogranite or quartz monzonite (Table 1). It has a trace element pattern with pronounced negative anomalies in Th, U, Nb–Ta, P and Ti, and positive anomalies in Sr, Zr–Hf and Eu (Fig. 5a, b), a highly fractionated REE pattern ($La_N/Yb_N = 110$) with low HREE contents (Yb = 0.036 ppm), and a strong positive Eu anomaly ($Eu/Eu^* = 11.0$). These features suggest derivation of the charnockite protolith through anatectic melting of country rocks during high-grade metamorphism.

The migmatized biotite gneisses (samples 6151, 6152 in Table 1) resemble rhyodacite and rhyolite (granodiorite and granite) in major element composition (Table 1). They have trace-element patterns enriched in Th and strongly depleted in HREE relative to the enderbites (Fig. 5a, b) as well as strongly fractionated REE patterns ($La_N/Yb_N = 81–106$) with weak Eu anomalies ($Eu/Eu^* = 1.06–1.14$). The chemical characteristics of the migmatized biotite gneisses require hornblende in the residue during derivation of their protoliths, implying higher pressures and, consequently, different sources than suggested for protoliths of the enderbites.

The biotite granite-gneiss (sample 6153), cutting the migmatites, has a granodioritic composition and geochemical characteristics similar to those of the migmatites but differs from these in its positive Sr anomaly, an absence of a Zr–Hf anomaly, and lower trace elements content (Fig. 5a, b).

5. Previous geochronology

U–Pb ID-TIMS dating of zircons from sample 6153 was performed in the Vernadsky Institute of Geochemistry and Analytical Chemistry, Russian Academy of Sciences for three multigrain zircon aliquots, with two fractions subjected to selective dissolution for 4 and 8 h, respectively. Analyses corresponding to the isotopic composition of the dated zircon fractions define a discordia line with an upper Concordia intercept at 2219 ± 25 Ma and a lower intercept at 535 ± 570 Ma, MSWD = 2.3. This age was considered to reflect the time of zircon crystallization and was interpreted as the upper age boundary for the Ider Complex (Kozakov et al., 2011). However, because of the multigrain dating method and no CL control, it is possible that the above discordia line reflects mixing between magmatic (or inherited) and metamorphic zircons. Therefore, the age of amphibolite-facies retrograde metamorphism in the Ider Complex remains uncertain.

6. Results and discussion

6.1. Zircon morphology, cathodoluminescence images, and U–Pb ages

Zircons from charnockite and enderbite samples 7011 and 7340 were analyzed on SHRIMP II of the Beijing SHRIMP Centre, and the analytical procedures are detailed in Appendix A. The analytical data are listed in Table 2.

Please cite this article as: Kröner, A., et al., Zircon ages and Nd–Hf isotopes in UHT granulites of the Ider Complex: A cratonic terrane within the Central Asian Orogenic Belt in..., Gondwana Research (2014), http://dx.doi.org/10.1016/j.gr.2014.03.005

Table 2
Major element composition of minerals from enderbite sample 7340 of the Ider Complex, northwestern Mongolia[a].
Mineral abbreviations after Kretz (1983).

Mineral	Opx	Opx	Opx	Opx	Opx	Opx	Opx	Bt	Bt	Bt	Bt	Bt	Bt
Spot	1	2	3	9	19	20	27	4	7	8	22	23	34
Notest								1	2	1	3	3	4
SiO_2	52.82	52.83	52.41	52.15	52.35	52.60	52.16	38.48	37.86	39.28	39.11	39.23	38.81
TiO_2	–	–	–	–	0.11	–	–	5.88	5.62	5.68	5.18	5.95	4.98
Al_2O_3	0.73	0.68	0.75	0.45	0.87	0.68	0.84	14.10	13.73	14.05	14.76	13.95	14.47
Cr_2O_3	–	–	–	–	–	–	–	0.31	0.09	0.21	0.26	0.35	0.20
FeO	25.92	26.06	26.30	26.74	25.98	26.53	26.18	17.40	18.16	16.71	16.35	16.63	16.77
MnO	0.61	0.59	0.50	0.65	0.44	0.43	0.75	0.11	0.08	0.10	0.03	–	–
MgO	19.10	19.18	19.18	19.39	19.35	19.15	19.25	13.01	13.08	13.03	13.41	13.01	14.65
CaO	0.82	0.65	0.71	0.63	0.90	0.62	0.82	–	0.47	0.20	0.02	0.10	0.14
Na_2O	–	–	0.14	–	–	–	–	0.10	0.40	0.17	0.12	0.12	0.09
K_2O	–	–	–	–	–	–	–	10.44	10.18	10.30	10.50	10.37	9.63
BaO	–	–	–	–	–	–	–	–	–	–	–	–	–
Cl	–	–	–	–	–	–	–	0.16	0.33	0.27	0.25	0.31	0.27
Total	100.00	99.99	99.99	100.01	100.00	100.01	100.00	99.99	100.00	100.00	99.99	100.02	100.01

Mineral	Or	Or	Or	Or	Or	Or	Pl	Pl	Pl	Pl	Pl	Pl	Pl	Pl
Spot	5	6	24	25	26	30	10	11	12	13	14	28	29	31
Notes	5	6	7	7	6	8								
SiO_2	62.86	63.25	63.13	62.42	62.67	63.10	58.43	58.41	58.41	58.31	58.66	59.36	58.94	58.76
TiO_2	–	–	–	–	–	–	–	–	–	–	–	–	–	–
Al_2O_3	19.84	19.66	19.56	20.06	19.61	19.74	26.86	26.79	26.12	26.61	26.21	25.89	26.09	26.04
Cr_2O_3	–	–	–	–	–	–	–	–	–	–	–	–	–	–
FeO	–	–	–	–	–	–	0.16	0.09	0.32	0.12	0.13	–	–	–
MnO	–	–	–	–	–	–	–	–	–	–	–	–	–	–
MgO	–	–	–	–	–	–	–	–	–	–	–	–	–	–
CaO	–	–	–	–	–	0.05	7.56	7.35	7.77	7.61	7.33	7.21	7.04	6.63
Na2O	0.49	0.73	0.41	0.36	0.46	0.43	6.82	7.18	7.18	6.98	7.28	7.11	7.53	6.51
K2O	15.85	15.45	15.98	16.21	15.93	15.86	0.18	0.17	0.20	0.37	0.40	0.42	0.41	2.06
BaO	0.95	0.92	0.92	0.95	1.11	0.81	–	–	–	–	–	–	–	–
Cl	–	–	–	–	–	–	–	–	–	–	–	–	–	–
Total	99.99	100.01	100.00	100.00	100.00	99.99	100.01	99.99	100.00	100.00	100.01	99.99	100.01	100.00

[a] Notes. 1 — mantled with Or; 2 — mica flake; 3 — ingrowth in Opx; 4 — secondary, in Opx grain; 5 — rim around a Bt grain; 6 — rim around a Opx grain; 7 — inclusion in anthipertite Pl; 8 — lamellae in anthipertite Pl.

Zircons from both samples are colorless and transparent, as is common in granulite-facies terrains (e.g., Kröner et al., 1994; Corfu et al., 2003). Both samples contain two morphologically distinct zircon generations. The more numerous grains are predominantly long-prismatic with length/width ratios of 3–6 and have well rounded terminations (e.g., Fig. 6a). Such rounding is known as metamorphic 'corrosion', i.e. partial zircon dissolution and recrystallization during high-grade metamorphism, and has been described from many metamorphic terranes (Silver, 1969; Kröner et al., 1994; Corfu et al., 2003). The predominantly dark CL images with frequent oscillatory zoning show these high-U zircons to be of magmatic origin (Fig. 6a–b). Some zircons have dark cores (Fig. 6b), and these are inherited as our isotopic data show. Several grains have thin metamorphic overgrowth rims (Fig. 6c) that, however, are too narrow to be analyzed on SHRIMP II with a 30 μm diameter ion beam. This thin overgrowth indicates that the charnockite was already dry during the high-grade event so that no or only very little zirconium-bearing fluid was available for new growth. Several grains of sample 7011 show complex internal structures under CL that, in analogy with similar zircons from other high-grade terranes, we interpret as the result of partial recrystallization (e.g., Fig. 6d), metamictization and other processes related to modifications as a result of interaction with a fluid phase (e.g., Wan et al., 2009). There are also rare low-U cores of magmatic origin and occasionally there occurs a complex intergrowth of low- and high-U phases (Fig. 6e). We avoided such zones during analysis and selected domains on the magmatic grains that indicated undisturbed growth.

The magmatic zircons in sample 7340 are generally less rounded at their terminations than those in 7011 and have simpler-looking internal structures (Fig. 6f), but many have very thin highly luminescent rims, too narrow to be analyzed on SHRIMP and most likely of metamorphic origin.

The second group of zircons in both samples is oval-shaped to ball-round, often multifaceted and very distinct because of their light gray highly luminescent CL images indicating low U-contents (Fig. 6g–i). These grains are undoubtedly of metamorphic origin. They often display typical fir-tree or sector zoning (Fig. 6g–h) due to slow diffusive growth during high-grade metamorphism under anhydrous conditions (e.g., Kröner et al., 2000; Wan et al., 2009; Dong et al., 2014). Some grains have older igneous-looking cores, in some instances just tiny domains (Fig. 7i), and some well-rounded grains, originally considered to be metamorphic turned out to be igneous in origin under CL (Fig. 6j). In general, the metamorphic zircons appear to have simpler internal structures than the igneous grains.

The heterogeneity of most zircons of igneous origin, as revealed by their CL images, clearly indicates that whole-grain isotopic analysis will not produce meaningful ages because several components are complexly intergrown in almost each grain and Pb-loss and/or recrystallization have most likely disturbed the original U–Pb isotopic ratios. A good example of such isotopic disturbance due to high-grade metamorphism is shown by Wan et al. (2011). In the ideal case of only two components, one magmatic and one metamorphic, the U–Pb isotopic ratios should define a discordia line in a Concordia diagram with the upper intercept approximating the magmatic crystallization age and the lower intercept reflecting new metamorphic growth and/or Pb-loss (e.g., Kröner et al., 2013b). As we demonstrate below, our zircons from the Ider Complex behave in exactly this way.

Eight grains of the igneous zircon population in sample 7011 were analyzed on SHRIMP II of which six yielded concordant or near-

Please cite this article as: Kröner, A., et al., Zircon ages and Nd–Hf isotopes in UHT granulites of the Ider Complex: A cratonic terrane within the Central Asian Orogenic Belt in..., Gondwana Research (2014), http://dx.doi.org/10.1016/j.gr.2014.03.005

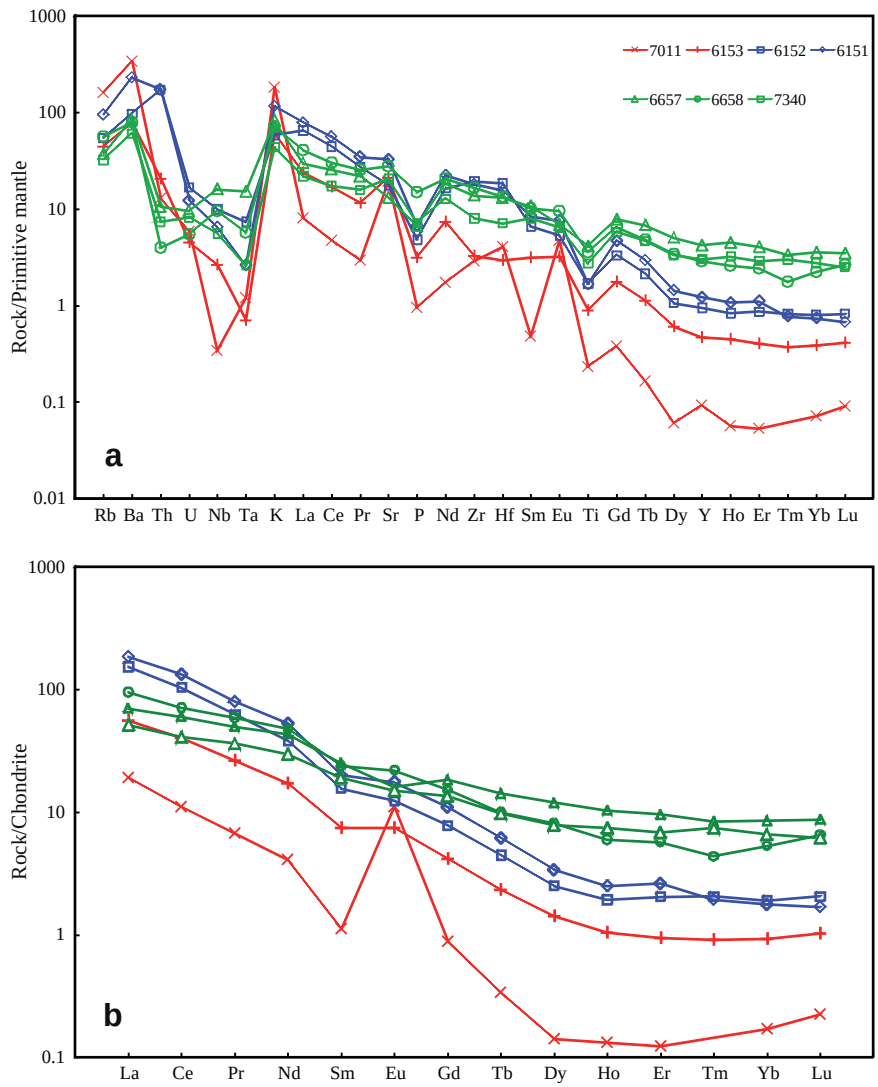

Fig. 5. (a) Primitive mantle-normalized trace-element variation diagram for rocks of the Ider Complex listed in Table 1. (b) Chondrite-normalized REE distribution patterns for rocks listed in Table 1.
Normalizing values are from Sun and McDonough (1989) and Taylor and McLennan (1985), respectively.

concordant results and two are significantly discordant (Fig. 7a), but all have similar $^{207}Pb/^{206}Pb$ isotopic ratios (Table 2) resulting in a mean age of 1855 ± 2 Ma (Fig. 7a). Three cores in the igneous zircons are much older but are strongly discordant and precise ages can therefore not be calculated. However, they are well aligned in the Concordia diagram and, as in their younger hosts, have near-identical $^{207}Pb/^{206}Pb$ ratios corresponding to a mean age of 2522 ± 2 Ma (Fig. 7a, inset). These cores most likely reflect the crustal source from which the charnockite protolith of sample 7011 was derived.

Five metamorphic zircons of sample 7011 produced concordant and near-concordant results (Table 2) with a mean $^{207}Pb/^{206}Pb$ age of 1857 ± 3 Ma (Fig. 7b) that we interpret to reflect the time of peak granulite-facies metamorphism. This age is identical, within error, to the age obtained on the magmatic grains, and there are two possibilities to interpret these results. First, and most likely, the granitic charnockite protolith crystallized at about 1855 Ma ago and resulted from melting of a late Archaean crustal source. High-grade metamorphism almost immediately followed on pluton emplacement and transformed the granite into a charnockite. Alternatively, all magmatic-looking zircons in this sample recrystallized completely during high-grade metamorphism, and their original isotopic system was totally reset. We consider the second option unlikely because some of the dated grains clearly preserve igneous oscillatory zoning and show no evidence in their CL-images of recrystallization.

Ten magmatic-looking zircons from sample 7340 yielded variably discordant but well aligned data with one concordant analysis, and the resulting mean $^{207}Pb/^{206}Pb$ age is 2542 ± 1 Ma (Table 2, Fig. 8a). We interpret this to reflect late Archaean crystallization of the enderbite protolith. Nine metamorphic zircons from the same sample have concordant, slightly discordant, and significantly discordant results but, as in sample 7011, their $^{207}Pb/^{206}Pb$ ratios are almost identical (Table 2) and result in a mean age of 1855 ± 3 Ma (Fig. 8b) which most likely reflects the peak of high-grade metamorphism. Two igneous cores in these zircons yielded discordant results suggesting a late Archaean minimum age of 2546 ± 1 Ma. This is identical to the magmatic age of sample 7340, as would be expected.

Comparing the two results it appears that sample 7340 represents a late Archaean basement that underwent late Paleoproterozoic granulite-facies metamorphism, whereas sample 7011 may reflect crustal melting of a late Archaean protolith in the late Paleoproterozoic, possibly the same basement as represented by sample 7340, immediately followed by high-grade metamorphism. Both samples experienced the same granulite-facies metamorphic event as recorded in their respective metamorphic zircons.

Please cite this article as: Kröner, A., et al., Zircon ages and Nd–Hf isotopes in UHT granulites of the Ider Complex: A cratonic terrane within the Central Asian Orogenic Belt in..., Gondwana Research (2014), http://dx.doi.org/10.1016/j.gr.2014.03.005

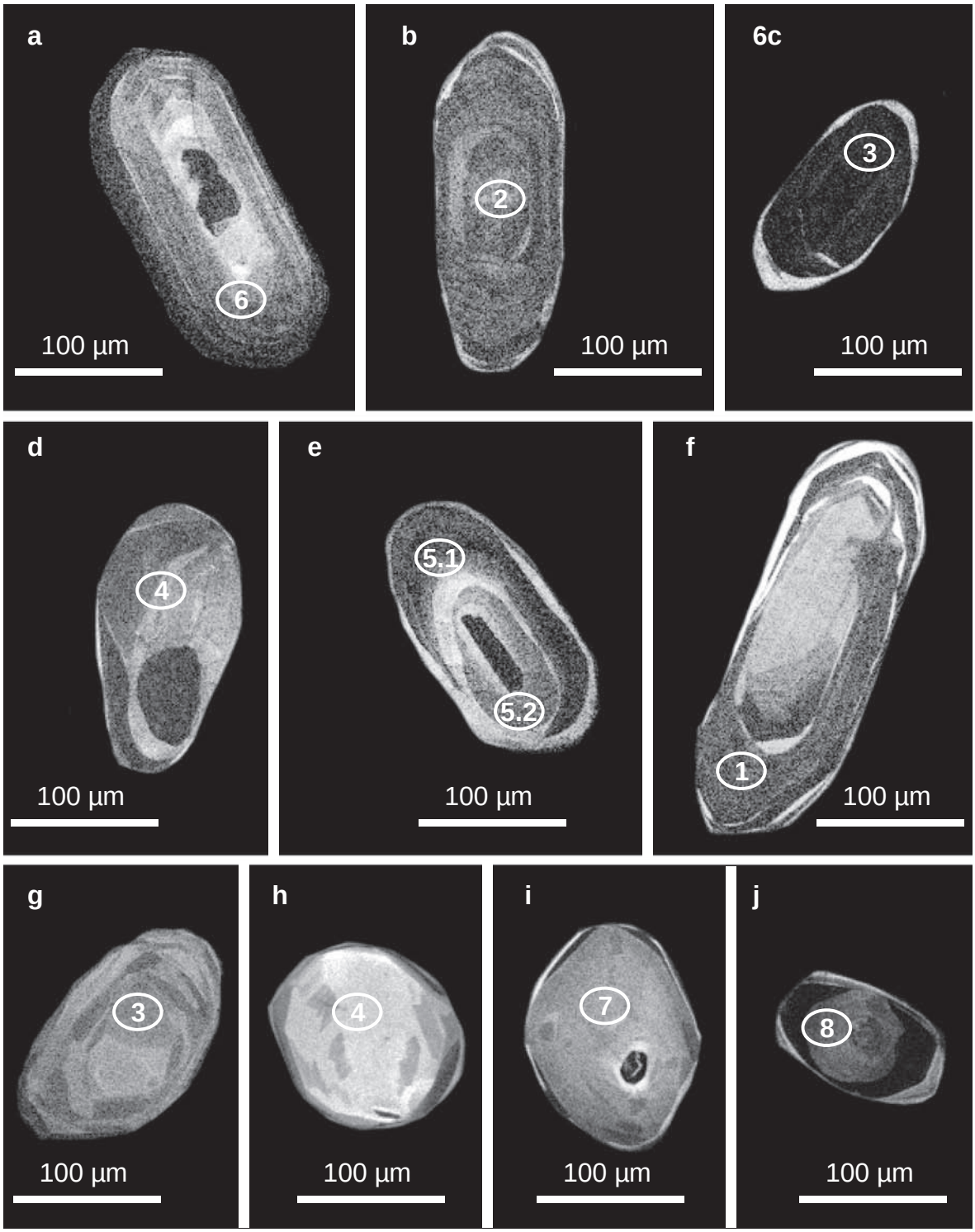

Fig. 6. Cathodoluminenscence images of zircons analyzed in this study. (a–e) Magmatic grains from charnockite sample 7011. (f) Magmatic grain from charnockite sample 7340. (g–h) Metamorphic zircons from sample 7011. (i) Metamorphic grain from sample 7340. (j) Well-rounded, translucent grain of seemingly metamorphic origin from sample 7340 but, in fact, igneous as shown by CL image and age. For explanation of the various features see text. SHRIMP analytical spots and numbers refer to Table 3.

6.2. Nd whole rock isotopic systematics

The Sm–Nd isotopic systematics of felsic igneous rocks are widely used to constrain their sources and the approximate time of crust formation from the depleted mantle (DePaolo, 1988). A sample is characterized by the $\varepsilon_{Nd(t)}$ parameter which denotes the initial Nd ratio at the time of rock formation. It is usually accepted that a positive $\varepsilon_{Nd(t)}$ value indicates a short-lived juvenile source, whereas a negative $\varepsilon_{Nd(t)}$ value is indicative of rock formation due to a reworking of a long-lived crustal source. The time of formation of a rock from a mantle source is calculated as the Nd model age $t_{Nd(DM)}$ that corresponds to the time when the Nd isotopic composition of this rock was identical to its mantle source. However, since felsic igneous rocks are often formed from sources with different isotopic compositions and ages, a Nd model age is usually interpreted as average crustal residence age and reflects the average age of the material involved in the formation of the rock

Please cite this article as: Kröner, A., et al., Zircon ages and Nd–Hf isotopes in UHT granulites of the Ider Complex: A cratonic terrane within the Central Asian Orogenic Belt in..., Gondwana Research (2014), http://dx.doi.org/10.1016/j.gr.2014.03.005

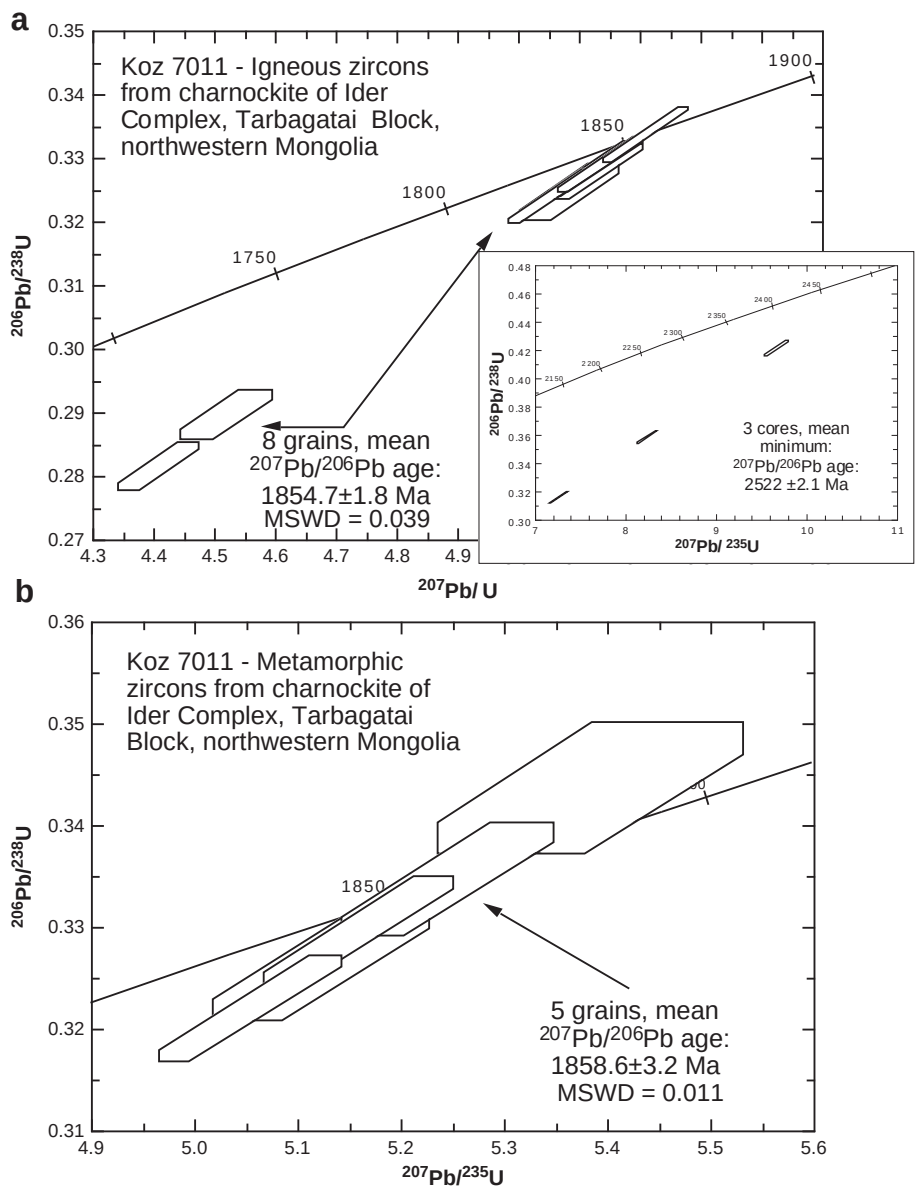

Fig. 7. Concordia diagrams showing analytical data for SHRIMP II analyses of zircons from charnockitic gneiss sample 7011 of the Ider Complex, Tarbagatai Block, northwestern Mongolia. Data boxes for each analysis are defined by standard errors in $^{207}Pb/^{235}U$, $^{206}Pb/^{238}U$ and $^{207}Pb/^{206}Pb$. For sample location see Fig. 3. (a) Magmatic zircons defining a mean age of 1855 ± 2 Ma; inset shows discordant position of Neoarchaean inherited cores. (b) Metamorphic zircons from the same sample defining a mean age of 1859 ± 3 Ma.

(Arndt and Goldstein, 1987). In spite of the generally immobile behavior of Sm and Nd during intracrustal processes (Taylor and McLennan, 1985), there are cases where anatexis of crustal rocks or fractionation of accessory minerals significantly changes the Sm/Nd ratio and thus leads to unrealistic $t_{Nd(DM)}$ estimates (e.g., Harris et al., 1996; Kovalenko et al., 1999). In order to account for such possible Sm–Nd fractionation, a so-called two-stage (or "crustal" by analogy with Hf-in-zircon isotope systematics; see below) Nd model age $t_{Nd(c)}$ (Keto and Jacobsen, 1987) can be calculated. This crustal Nd model age assumes that the average crustal Sm/Nd ratio for a potential source evolved from the time of depleted mantle melting to the age of rock crystallization. We use such crustal model ages below.

Nd whole-rock isotopic data for whole-rock samples of the Ider Complex are summarized in Table 4 and compared with Nd isotopic data for gneisses and Paleoproterozoic granitoids of the Baidarik Block in Fig. 9. Enderbites of the Ider Complex have slightly negative and close to zero $\varepsilon_{Nd(t)}$ values varying from −1.8 to +0.4 and corresponding Mesoarchaean Nd depleted mantle model ages $t_{Nd(DM)}$ of 3.1–2.9 Ga. The Nd isotopic and geochemical data suggest derivation of the enderbite precursors from melting of late Archaean juvenile as well as older crustal sources, probably in an active continental margin setting.

The migmatized biotite gneisses yielded higher positive $\varepsilon_{Nd(t)}$ values of +1.5 to +1.6, assuming a rock formation age of 2540 Ma. The remaining migmatized gneisses as well as a granite-gneiss and charnockite have low $^{147}Sm/^{144}Nd$ ratios of 0.0561–0.0733, much lower than average crustal values of 0.09–0.13, and this may have been caused by migmatization and anatexis. The corresponding Nd crustal model ages $t_{Nd(c)}$ of 2.8–2.5 Ga are strongly dependent on the assumed crystallization age. The Nd crustal model ages $t_{Nd(c)}$ of 2.8 Ga for the migmatized gneisses are close to depleted mantle model ages $t_{Nd(DM)}$ for the enderbites, suggesting that both crustal reworking and input of some juvenile material occurred during generation of the migmatite precursors.

The granite-gneiss and charnockite are characterized by negative $\varepsilon_{Nd(t)}$ values of −4.5 and −7.6, corresponding to Mesoarchaean crustal

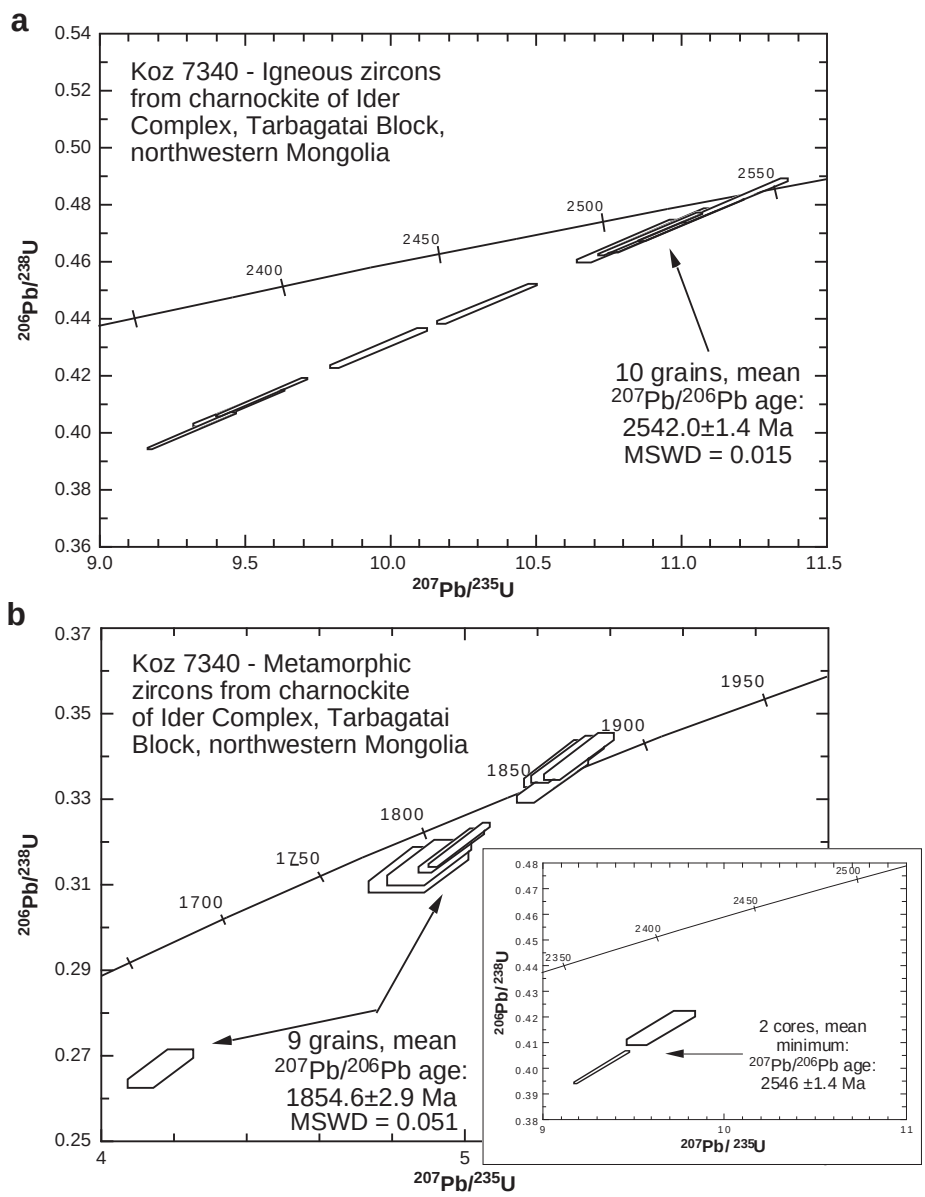

Fig. 8. Concordia diagrams showing analytical data for SHRIMP II analyses of zircons from charnockitic gneiss sample 7340 of the Ider Complex, Tarbagatai Block, northwestern Mongolia. Data boxes and sample location as in Fig. 7(a) Magmatic zircons defining a mean age of 2543 ± 1 Ma. (b) Metamorphic zircons from the same sample defining a mean age of 1855 ± 3 Ma. Inset shows inherited cores with Neoarchaean minimum ages.

Nd model ages $t_{Nd(c)}$ of 3.0 Ga. These rocks are similar in their Nd isotopic evolution to enderbites and migmatized gneisses of the Ider Complex (Fig. 9). The Nd isotope and geochemical data imply derivation of the charnockite and granite-gneiss precursors through anatexis of older crustal rocks.

Rocks of the Ider Complex have Nd model ages that partly overlap with, but are generally younger than, 3.3–2.9 Ga model ages for metamorphic rocks of the Baidarik Block (Fig. 9). This is probably related to the addition of juvenile material at ca. 2540 Ma.

6.3. Hf isotopic systematics

Hf isotopic ratios were obtained on previously dated SHRIMP spots and additional domains on zircons from samples 7011 and 7340, using a Nu Plasma HR MC-ICP-MS equipped with a laser ablation system at the University of Hong Kong (for analytical details see Appendix A). The results are summarized in Table 5.

The isotopic ratios in all zircons are remarkably similar, attesting to the robustness of the Lu–Hf system, even in cases of significant Pb-loss in the zircons during metamorphism. It is possible to calculate an approximate age for the source rock from which the zircons were derived, namely a Hf crustal model age (t_{Hfc}), by forcing a growth curve for a system with a Lu/Hf isotopic ratio corresponding to the average crust through the zircon initial ratio. However, there is some uncertainty in the calculation of this model age because the whole-rock $^{176}Lu/^{177}Hf$ ratio of the protolith is not known, and therefore most authors use an assumed value for the continental crust, varying between 0.009 and 0.015 (e.g., Vervoort and Patchett, 1996; Belousova et al., 2006). Whole-rock Lu–Hf isotopic data from a wide variety of high-grade granitoid gneisses suggest that a ratio of 0.010 appears to be most suitable and also best matches whole-rock Nd model ages (Kröner et al., 2013a, 2014). However, we caution against taking these values too literally because the real Lu/Hf protolith ratios are not known, and there is also some uncertainty on the degree of depletion of the average

Please cite this article as: Kröner, A., et al., Zircon ages and Nd–Hf isotopes in UHT granulites of the Ider Complex: A cratonic terrane within the Central Asian Orogenic Belt in..., Gondwana Research (2014), http://dx.doi.org/10.1016/j.gr.2014.03.005

Table 3
SHRIMP II analytical data for spot analyses of igneous and metamorphic zircons from high-grade rocks of the Ider Complex, Tarbagatai Block, northwestern Mongolia.

Sample no.	U ppm	Th ppm	Th/U	$^{206}Pb/^{204}Pb$	$^{208}Pb/^{206}Pb$	$^{207}Pb/^{206}Pb$	$^{206}Pb/^{238}U$	$^{207}Pb/^{235}U$	206/238 Age ± 1σ	207/235 Age ± 1σ	207/206 Age ± 1σ
Koz7011-1	936	50	0.053	44,405	0.0156 ± 3	0.1133 ± 3	0.3242 ± 42	5.065 ± 70	1810 ± 21	1830 ± 12	1853 ± 5
Koz7011-2	677	120	0.177	30,276	0.0437 ± 4	0.1663 ± 5	0.4221 ± 56	9.678 ± 133	2270 ± 25	2405 ± 13	2521 ± 5
Koz7011-3	1187	52	0.044	63,492	0.0129 ± 2	0.1134 ± 3	0.3340 ± 44	5.222 ± 71	1858 ± 21	1856 ± 12	1855 ± 4
Koz7011-4.1	1035	81	0.078	118,765	0.0238 ± 3	0.1134 ± 3	0.3291 ± 43	5.148 ± 71	1834 ± 21	1844 ± 12	1855 ± 5
Koz7011-4.2	526	29	0.055	46,512	0.0166 ± 4	0.1137 ± 5	0.3282 ± 43	5.144 ± 74	1830 ± 21	1843 ± 12	1859 ± 7
Koz7011-5.1	883	49	0.055	26,838	0.0156 ± 4	0.1133 ± 4	0.3286 ± 43	5.134 ± 71	1832 ± 21	1842 ± 12	1853 ± 6
Koz7011-5.2	4867	1042	0.214	18,911	0.0585 ± 2	0.1664 ± 2	0.3165 ± 41	7.264 ± 96	1773 ± 20	2144 ± 12	2522 ± 2
Koz7011-6	209	1	0.005	9080	0.0013 ± 11	0.1137 ± 9	0.3249 ± 44	5.096 ± 83	1814 ± 21	1835 ± 14	1860 ± 14
Koz7011-7.1	1479	287	0.194	32,584	0.0459 ± 3	0.1663 ± 3	0.3595 ± 47	8.245 ± 111	1980 ± 22	2258 ± 12	2521 ± 3
Koz7011-7.2	198	100	0.505	6732	0.1488 ± 20	0.1132 ± 9	0.2899 ± 39	4.524 ± 77	1641 ± 20	1735 ± 14	1851 ± 16
Koz7011-8	654	35	0.054	3613	0.0186 ± 12	0.1136 ± 7	0.2818 ± 37	4.412 ± 66	1600 ± 19	1715 ± 12	1857 ± 11
Koz7011-9	8496	671	0.079	121,359	0.0251 ± 11	0.1216 ± 1	0.1327 ± 17	2.225 ± 29	803 ± 10	1189 ± 9	1980 ± 2
Koz7011m-1	35	5	0.143	11,387	0.0566 ± 33	0.1136 ± 21	0.3438 ± 65	5.384 ± 149	1905 ± 31	1882 ± 24	1858 ± 33
Koz7011m-2	130	<1	<0.008	12,784	0.0070 ± 15	0.1138 ± 11	0.3266 ± 55	5.123 ± 105	1822 ± 27	1840 ± 17	1861 ± 17
Koz7011m-3	399	2	0.005	140,252	0.0031 ± 4	0.1138 ± 5	0.3222 ± 52	5.054 ± 88	1800 ± 26	1828 ± 15	1861 ± 9
Koz7011m-4	176	1	0.006	11,442	0.0035 ± 15	0.1136 ± 10	0.3348 ± 56	5.246 ± 103	1862 ± 27	1860 ± 17	1858 ± 16
Koz7011m-5	305	3	0.010	25,075	0.0039 ± 7	0.1135 ± 6	0.3298 ± 54	5.159 ± 92	1837 ± 26	1846 ± 15	1855 ± 10
Koz7340-1	555	82	0.148	40,717	0.0417 ± 5	0.1685 ± 5	0.4707 ± 76	10.934 ± 183	2486 ± 33	2518 ± 15	2543 ± 5
Koz7340-2	956	245	0.256	13,742	0.0714 ± 4	0.1687 ± 4	0.4744 ± 76	11.035 ± 182	2503 ± 33	2526 ± 15	2545 ± 4
Koz7340-3	1210	215	0.178	93,371	0.0481 ± 3	0.1686 ± 3	0.4811 ± 77	11.185 ± 183	2532 ± 34	2539 ± 15	2544 ± 3
Koz7340-4	892	170	0.191	14,432	0.0543 ± 4	0.1683 ± 4	0.4086 ± 66	9.481 ± 157	2209 ± 23	2386 + 15	2541 ± 4
Koz7340-5	758	606	0.799	19,581	0.2309 ± 8	0.1682 ± 6	0.4294 ± 69	9.962 ± 166	2303 ± 31	2431 ± 15	2540 ± 4
Koz7340-6	245	216	0.882	4392	0.2480 ± 13	0.1682 ± 2	0.4668 ± 75	10.826 ± 185	2470 ± 33	2508 ± 16	2540 ± 6
Koz7340-7	1212	63	0.052	31,133	0.0125 ± 2	0.1682 ± 2	0.4122 ± 66	9.559 ± 156	2225 ± 30	2393 ± 15	2540 ± 2
Koz7340-8	689	241	0.350	14,995	0.0950 ± 6	0.1684 ± 4	0.4451 ± 72	10.333 ± 172	2373 ± 32	2465 ± 15	2542 ± 4
Koz7340-9	1219	284	0.233	47,574	0.0648 ± 2	0.1683 ± 2	0.4693 ± 75	10.894 ± 177	2481 ± 33	2514 ± 15	2541 ± 2
Koz7340-10	861	90	0.105	29,603	0.0281 ± 3	0.1687 ± 3	0.4006 ± 64	9.317 ± 153	2172 ± 30	2370 ± 15	2545 ± 3
Koz7340m-1	108	1	0.009	3432	0.0012 ± 29	0.1130 ± 16	0.3151 ± 53	4.908 ± 115	1766 ± 26	1804 ± 20	1848 ± 26
Koz7340m-2	91	1	0.011	4624	0.0028 ± 21	0.1132 ± 12	0.3382 ± 56	5.277 ± 110	1878 ± 27	1865 ± 18	1851 ± 20
Koz7340m-3	214	1	0.005	9656	0.0050 ± 12	0.1138 ± 8	0.3343 ± 55	5.246 ± 99	1859 ± 26	1860 ± 16	1861 ± 13
Koz7340m-4	179	1	0.006	10,498	0.0026 ± 9	0.1133 ± 7	0.3179 ± 52	4.967 ± 90	1780 ± 25	1814 ± 15	1853 ± 11
Koz7340m-5	117	<1	<0.009	3798	0.0035 ± 24	0.1133 ± 14	0.2668 ± 44	4.170 ± 90	1525 ± 22	1668 ± 18	1854 ± 22
Koz7340m-6	49	<1	<0.020	1693	0.0035 ± 46	0.1130 ± 23	0.3133 ± 53	4.879 ± 137	1757 ± 26	1799 ± 24	1848 ± 37
Koz7340m-7	252	1	0.004	9973	0.0014 ± 10	0.1136 ± 7	0.3397 ± 55	5.320 ± 97	1885 ± 27	1872 ± 16	1857 ± 11
Koz7340m-8	494	10	0.020	26,525	0.0056 ± 5	0.1135 ± 4	0.3191 ± 51	4.992 ± 85	1785 ± 25	1818 ± 14	1856 ± 7
Koz7340m-9	98	83	0.847	3003	0.2409 ± 31	0.1683 ± 3	0.4160 ± 69	9.652 ± 190	2242 ± 31	2402 ± 18	2541 ± 15
Koz7340m-10	861	90	0.105	42,052	0.0284 ± 3	0.1688 ± 3	0.4006 ± 64	9.325 ± 153	2172 ± 30	2370 ± 15	2546 ± 3
Koz7340m-3.2	222	1	0.005	7933	0.0024 ± 11	0.1130 ± 8	0.3393 ± 55	5.287 ± 97	1883 ± 27	1867 ± 16	1848 ± 12

Koz7011-1 is spot on grain 1, Koz7011-2 is spot on grain 2, etc.

Archaean mantle. Thus the error in the Hf crustal model ages cited below may be considerable.

The Hf initial ratios for six of the 1855 Ma zircons from sample 7011, expressed in ε_{Hf}-units, are between −9.0 and −5.7 (Table 5, Fig. 10a). Four analyses were made on zircon cores of which three had a measured mean age of 2522 Ma, and we assume that the remaining core has approximately the same age. The $\varepsilon_{Hf(t)}$-values for these old cores range between −3.6 and −0.3 (Table 4). These data are graphically shown in Fig. 10a where the Hf initial ratios at the time of rock formation (1855 Ma for the magmatic grains, 2522 Ma for the inherited cores, see Table 5) are plotted against time. The red broken lines denote the evolution of the Hf isotopic ratios for the highest and lowest $\varepsilon_{Hf(t)}$-values, assuming a $^{176}Lu/^{177}Hf$ ratio of 0.01. For the magmatic zircons of sample 7011 the resulting t_{Hfc} crustal model ages vary between 2.7 and 2.9 Ga, whereas the Neoarchaean cores have model ages of 2.9–3.1 Ga (Table 5, Fig. 10a). The latter are just slightly older than those for the Paleoproterozoic magmatic grains and support the interpretation that both the charnockite precursor of sample 7011 and its possible igneous source represented by the zircon cores, were derived from Neo- to Mesoarchaean crustal material.

Nine Lu–Hf analyses of metamorphic zircons from sample 7011, calculated for an age of 1857 Ma, yielded strongly negative $\varepsilon_{Hf(t)}$-values ranging between −19.2 and −11.2 and corresponding t_{Hfc} model ages of ca. 3.0–3.4 Ga (Table 5, Fig. 10b). These old model ages are close to those of the igneous zircons and suggest that the Lu–Hf isotopic system has been inherited from the magmatic source and was not significantly disturbed by the high-grade metamorphic event.

The Hf initial ratios for ten magmatic zircons from sample 7340, calculated for a crystallization age of 2542 Ma, vary widely between −5.0 and +2.7 and resulting in Hf crustal model ages of 2.8 to 3.2 Ga (Table 5,

Table 4
Sm–Nd whole-rock isotopic data for rocks of the Ider Complex, northwestern Mongolia.

Sample no.	Age, Ma	Sm, ppm	Nd, ppm	$^{147}Sm/^{144}Nd$	$^{143}Nd/^{144}Nd$ ($\pm 2\sigma_m$)	$\varepsilon_{Nd}(0)$	$\varepsilon_{Nd}(t)$	$t_{Nd(DM)}$	$t_{Nd(C)}$
7011	1855	0.22	2.37	0.0561	0.510532 ± 4	−41.1	−7.6	2520	2972
6153	2219	1.44	10.92	0.0797	0.510698 ± 9	−37.8	−4.5	2776	3013
6151	2540	3.76	20.07	0.0685	0.510570 ± 3	−40.3	1.6	2695	2778
6152	2540	2.75	22.64	0.0733	0.510647 ± 2	−38.8	1.5	2705	2785
6657	2540	4.97	25.01	0.1202	0.511369 ± 4	−24.8	0.2	2888	2888
6658	2540	4.74	27.93	0.1025	0.511042 ± 2	−31.1	−0.4	2874	2937
7340	2540	3.29	16.19	0.1229	0.511313 ± 2	−25.8	−1.8	3067	3051

Please cite this article as: Kröner, A., et al., Zircon ages and Nd–Hf isotopes in UHT granulites of the Ider Complex: A cratonic terrane within the Central Asian Orogenic Belt in..., Gondwana Research (2014), http://dx.doi.org/10.1016/j.gr.2014.03.005

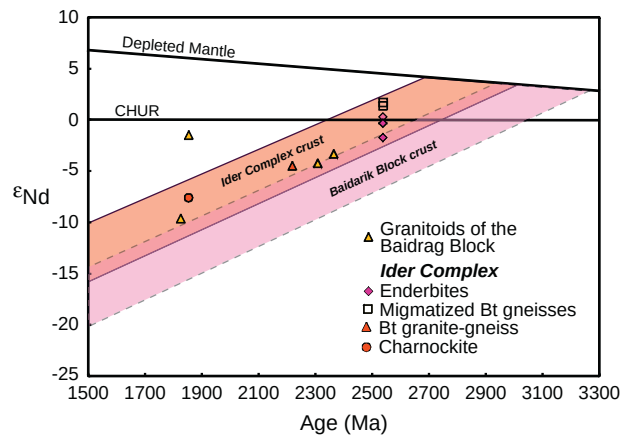

Fig. 9. ε_{Nd} versus age diagram for gneisses of the Ider Complex in comparison with gneisses and granitoids of the Baidarik Block.
Data from Kozakov et al. (1997) and Kozakov et al. (2011) and Table 3.

Fig. 10c), very similar to the zircon cores of charnockite sample 7011. This suggests that these cores probably represent the same crustal material as represented by sample 7340. Ten Lu–Hf analyses of metamorphic zircons from sample 7340 yielded extremely variable $e_{Hf(t)}$-values ranging from −18.5 to −5.4 if calculated for a metamorphic age of 1855 Ma. Two of these have very low values of −15.5 and −18.5, and we suspect that these grains contain inherited material of possible Archaean age not visible in CL images but shown in some of the metamorphic zircons of this population (see Fig. 7f). It is therefore possible that the laser beam cut deeply into these zircons and evaporated an Archaean or mixed phase. If we calculate crustal model ages for these two samples on the basis of a crystallization at 2542 Ma (Table 5) and combine these with the remaining $e_{Hf(t)}$-values for the metamorphic grains, the range is between −10.0 and +0.1 (Fig. 10d), corresponding to t_{Hfc} model ages of 2.7 to 3.1 Ga which are again similar to those in the igneous zircons of the same sample and reiterate the suggestion that the Lu–Hf isotopic system of the metamorphic zircons is inherited from the magmatic enderbite protolith.

We suggest that this occurred in the following manner. Igneous zircon becomes "corroded" through the action of a fluid phase and partly dissolves during prograde high-temperature metamorphism. This can be seen in many zircons from high-grade terranes where the original pyramidal terminations of magmatic zircons are lost and become well rounded and "healed" as evidenced by multifaceted surfaces seen under high microscopic magnification (e.g., Kröner et al., 2013b). Such dissolution may also result in unusual zircon shapes (e.g., Fig.7d), including egg- or even ball-shaped grains (e.g., Fig. 7e) that are easily mistaken for detrital zircon. The dissolved material bearing the Hf isotopic composition of the "parent" igneous zircon is transported in the

Table 5
Lu–Hf isotopic data for igneous and metamorphic zircons from high-grade gneisses of the Ider Complex, Tarbgatai Block, northwestern Mongolia[a].

Sample, spot	t (Ma)	$^{176}Yb/^{177}Hf$	±1σ	$^{176}Lu/^{177}Hf$	±1σ	$^{176}Hf/^{177}Hf$	±1σ	$(^{176}Hf/^{177}Hf)i$	εHf(t)	±1σ	tc (Ga)	±1σ
KOZ7011-1	1855	0.003445	0.000053	0.000157	0.000003	0.281368	0.000012	0.281363	−8.55	0.42	2.86	0.02
KOZ7011-2	2522	0.017506	0.000222	0.000855	0.000012	0.281173	0.000014	0.281132	−1.47	0.49	3.03	0.03
KOZ7011-3	1855	0.002975	0.000020	0.000135	0.000001	0.281355	0.000012	0.281350	−8.98	0.42	2.88	0.02
KOZ7011-4	1855	0.009308	0.000163	0.000465	0.000009	0.281397	0.000018	0.281381	−7.90	0.63	2.83	0.03
KOZ7011-5	1855	0.003215	0.000025	0.000150	0.000002	0.281449	0.000010	0.281444	−5.66	0.35	2.71	0.02
KOZ7011-6-1	1855	0.003151	0.000012	0.000148	0.000001	0.281406	0.000011	0.281401	−7.19	0.35	2.79	0.02
KOZ7011-6.2	2522	0.030158	0.000094	0.001564	0.000005	0.281150	0.000013	0.281075	−3.50	0.42	3.14	0.02
KOZ7011-7	2522	0.000942	0.000011	0.000050	0.000001	0.281210	0.000009	0.281208	1.23	0.32	2.89	0.02
KOZ7011-8	2522	0.027078	0.000182	0.001387	0.000010	0.281202	0.000012	0.281135	−1.35	0.42	3.02	0.03
KOZ7011-9	2522	0.003849	0.000056	0.000191	0.000003	0.281174	0.000017	0.281165	−0.29	0.60	2.97	0.03
KOZ7011-10-1	1855	0.002975	0.000042	0.000149	0.000003	0.281372	0.000011	0.281367	−8.40	0.39	2.85	0.02
KOZ7011-10-2	2522	0.039147	0.000064	0.001999	0.000003	0.281169	0.000010	0.281073	−3.57	0.35	3.14	0.02
KOZ7011-11	2522	0.025802	0.000103	0.001320	0.000006	0.281170	0.000012	0.281106	−2.37	0.42	3.09	0.02
KOZ7011m-1	1857	0.000517	0.000003	0.000023	0.000000	0.281226	0.000009	0.281225	−13.40	0.28	3.11	0.02
KOZ7011m-2	1857	0.000510	0.000008	0.000033	0.000001	0.281121	0.000009	0.281119	−17.14	0.32	3.31	0.01
KOZ7011m-3	1857	0.000112	0.000002	0.000006	0.000000	0.281062	0.000021	0.281061	−19.20	0.73	3.41	0.04
KOZ7011m-4	1857	0.000946	0.000022	0.000045	0.000001	0.281247	0.000013	0.281245	−12.68	0.46	3.08	0.02
KOZ7011m-5	1857	0.000568	0.000002	0.000026	0.000000	0.281177	0.000010	0.281176	−15.14	0.35	3.20	0.02
KOZ7011m-7	1857	0.000445	0.000005	0.000028	0.000001	0.281183	0.000009	0.281182	−14.93	0.32	3.19	0.02
KOZ7011m-8	1857	0.000144	0.000003	0.000007	0.000000	0.281256	0.000007	0.281255	−12.31	0.25	3.06	0.01
KOZ7011m-9	1857	0.000400	0.000004	0.000017	0.000000	0.281289	0.000010	0.281288	−11.15	0.35	3.00	0.02
KOZ7011m-10	1857	0.000706	0.000026	0.000036	0.000001	0.281237	0.000009	0.281235	−13.02	0.32	3.09	0.02
KOZ7340-1	2542	0.008743	0.000023	0.000398	0.000001	0.281180	0.000012	0.281161	0.03	0.42	2.97	0.02
KOZ7340-2	2542	0.012252	0.000052	0.000572	0.000002	0.281148	0.000012	0.281121	−1.41	0.39	3.04	0.02
KOZ7340-3	2542	0.011987	0.000040	0.000578	0.000002	0.281182	0.000011	0.281154	−0.21	0.35	2.98	0.02
KOZ7340-4	2542	0.016641	0.000048	0.000794	0.000002	0.281210	0.000011	0.281172	0.42	0.35	2.95	0.02
KOZ7340-5	2542	0.021728	0.000124	0.000964	0.000006	0.281166	0.000013	0.281120	−1.44	0.46	3.04	0.02
KOZ7340-6	2542	0.024603	0.000134	0.001059	0.000005	0.281141	0.000012	0.281090	−2.50	0.42	3.10	0.02
KOZ7340-7	2542	0.011274	0.000070	0.000579	0.000004	0.281200	0.000011	0.281172	0.43	0.35	2.95	0.02
KOZ7340-8	2542	0.032641	0.000229	0.001333	0.000009	0.281084	0.000011	0.281020	−5.00	0.39	3.23	0.02
KOZ7340-9	2542	0.014582	0.000019	0.000670	0.000001	0.281180	0.000012	0.281148	−0.44	0.39	2.99	0.02
KOZ7340-10	2542	0.020914	0.000111	0.000839	0.000004	0.281277	0.000008	0.281237	2.72	0.28	2.82	0.02
KOZ7340m-1	1855	0.000729	0.000011	0.000023	0.000001	0.281410	0.000008	0.281410	−6.88	0.25	2.77	0.01
KOZ7340m-2	1855	0.000380	0.000006	0.000013	0.000000	0.281452	0.000010	0.281452	−5.38	0.35	2.69	0.02
KOZ7340m-3	1855	0.000808	0.000008	0.000029	0.000001	0.281345	0.000010	0.281344	−9.20	0.32	2.89	0.02
KOZ7340m-4	2542	0.001195	0.000038	0.000039	0.000002	0.281084	0.000020	0.281082	−2.69	0.71	3.11	0.04
KOZ7340m-5	1855	0.000880	0.000011	0.000035	0.000001	0.281366	0.000015	0.281364	−8.48	0.54	2.86	0.03
KOZ7340m-6	1855	0.000646	0.000008	0.000022	0.000001	0.281397	0.000010	0.281397	−7.34	0.35	2.80	0.02
KOZ7340m-7	1855	0.001119	0.000009	0.000048	0.000001	0.281322	0.000010	0.281321	−10.04	0.35	2.94	0.02
KOZ7340m-8	1855	0.000855	0.000009	0.000034	0.000001	0.281347	0.000013	0.281346	−9.13	0.46	2.89	0.02
KOZ7340m-9	2542	0.012515	0.000584	0.000545	0.000025	0.281187	0.000017	0.281161	0.12	0.58	2.96	0.03
KOZ7340m-10	1855	0.000417	0.000003	0.000013	0.000000	0.281418	0.000011	0.281418	−6.58	0.39	2.76	0.02

[a] Koz7011-6-1 is grain 6, spot 1, Koz7011-6-2 is grain 6, spot 2, etc.; m denotes metamorphic zircon.

Please cite this article as: Kröner, A., et al., Zircon ages and Nd–Hf isotopes in UHT granulites of the Ider Complex: A cratonic terrane within the Central Asian Orogenic Belt in..., Gondwana Research (2014), http://dx.doi.org/10.1016/j.gr.2014.03.005

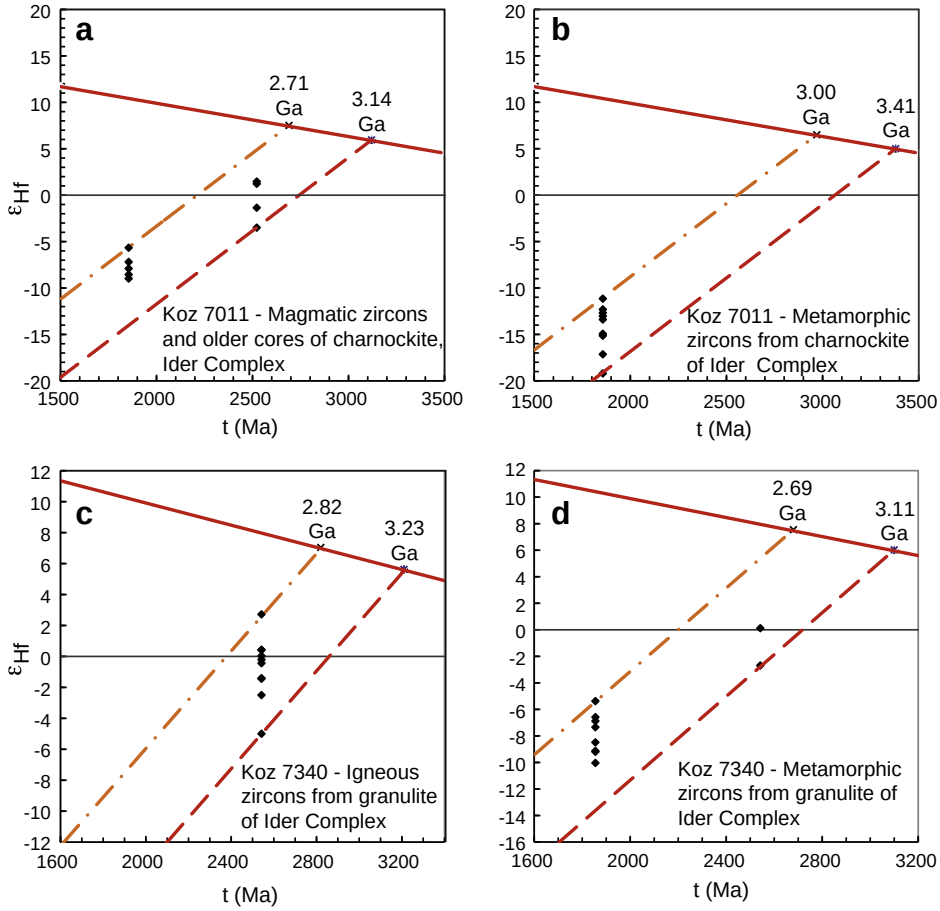

Fig. 10. Hf evolution diagrams showing analytical data and Hf_c model ages for zircons from charnockites of the Ider Complex, Tarbagatai Block, northwestern Mongolia. The broken Hf evolution lines are based on $^{176}Lu/^{177}Hf = 0.01$. (a) Magmatic zircons and inherited cores in sample 7011. (b) Metamorphic zircon in the same sample. (c) Magmatic zircons in sample 7340. (d) Metamorphic zircon in the same sample. (For interpretation of the references to color in this figure, the reader is referred to the web version of this article.)

metamorphic fluid that, under suitable conditions, leads to the crystallization of new metamorphic zircon in the rock. This newly-formed zircon, characterized by a typical ball-round, multifaceted shape, broad zoning as revealed under CL, and a low Th/U ratio, as seen in our samples, then has a new U–Th–Pb isotopic system reflecting the time of metamorphic crystallization, but it inherited the Hf isotopic composition from the fluid from which it nucleated. A similar process was envisaged by Zeh et al. (2010) for Hf isotopes in metamorphic zircon from amphibolite-facies schists in Antarctica and in eclogite-facies rocks from the Dabie orogen, China. Zeh et al. (2010) suggested that the dissolution/transportation/re-precipitation process resulted from a complex interplay between metamorphic dehydration reactions and synmetamorphic deformation processes.

7. Conclusions

The results of our study on high-grade rocks from the Ider Complex of northwestern Mongolia are summarized as follows:

1. The Ider Complex of the Tarbagatai Block in northwestern Mongolia contains high-grade granitoid gneisses with protolith ages of ca. 2550 Ma.
2. These late Archaean rocks (enderbites and two-pyroxene gneisses) have undergone UHT granulite-facies metamorphism at ca. 1850 Ma, followed by a retrogressive and amphibolite-facies overprint. Similar ages have been obtained for granulites of the Baidaragin Complex (protolith emplacement ages of 2.65–2.44 Ga, Kozakov et al., 2007) and intrusion of a Grt ± Opx bearing syntectonic granodiorite at 1854 ± 5 Ma (Kozakov, 1993).
3. Nd whole-rock isotopic systematics with Nd model ages ranging between ca. 2.5 and 3.1 Ga suggest that both crustal reworking and input of some juvenile material were involved in the generation of the Ider Complex gneiss protholiths. Hf-in-zircon isotopic data provide a similar pattern, and magmatic zircon also yielded Archaean Hf crustal model ages. The metamorphic zircon population seems to have inherited its Hf isotopic composition from the igneous grains, suggesting a complex process of dissolution, transportation, and re-precipitation involving a fluid phase during high-grade metamorphism.
4. Current data show that only three relatively small crustal blocks containing early Precambrian high-grade rocks occur in the eastern segment of the CAOB, namely the Baidrag, Ider and Gargan complexes. Other supposed microcontinents in the region are Neoproterozoic in age.
5. The zircon age patterns for the two samples of the Ider Complex do not make it possible to unambiguously assign the Tarbagatai Block to any of the cratons bordering the Central Asian Orogenic Belt, since age peaks at ca. 2520–2550 and ca. 1860 Ma are common in the Siberian, North China and Tarim cratons (Rojas-Agramonte et al., 2011).

Acknowledgments

Liqin Zhou and Xiao-chao Che of the Beijing SHRIMP Centre provided the zircon CL images, Chun Yang prepared a perfect zircon mount, and Zhiqing Yang and Jianhui Liu tuned the SHRIMP instrument for perfect analyses. Xie Hangqiang kindly assisted in the SHRIMP analyses. Work in the Nd isotope laboratory in St. Petersburg was assisted by

L.B. Terent'eva. Jianfeng Gao of the Geological Survey of Canada provided an unpublished Excel-based program to construct the Hf evolution diagrams of Fig. 10, and Figs. 1–3 were drawn by G.P. Pleskach. This research was supported by the Russian Foundation for Basic Research (RFBR grants 11-05-92003 and 14-05-00208) and is also part of a collaborative study between Mainz University and The University of Hong Kong, funded jointly by the Hong Kong Research Grants Council (RGC 704712P) and the DAAD/RGC Germany/Hong Kong Joint Research Scheme (G HK033/12 and PPP).

Appendix A. Sample preparation and analytical procedures

Major element abundances were determined using XRF methods in the Institute of the Earth's Crust, Siberian Branch, Russian Academy of Sciences (RAS), Irkutsk. The detailed analytical procedures are described in Afonin et al. (1992). *Trace elements and REE concentrations* were determined on a VG Elemental PlasmaQuad PQ2 + "Turbo" inductively-coupled plasma mass spectrometer (ICP-MS) after lithium metaborate fusion. The analytical procedures were described by Panteeva et al. (2003). Standard reference materials were BHVO-2 (basalt), RGM-1 (ryolite), W-2 (diabase), JG-2 and G-2 (granites). The precision is better than 10%.

Mineral analyses from enderbite sample 7340 were performed on a JEOL JSM-6510LA electron microscope equipped with a JED-2200 analyzer at the Institute of Precambrian Geology and Geochronology, St. Petersburg, using a 20 kV accelerating voltage. Counting times for peak and background intensities were 30 s. Calibration was carried out with a set of artificial and natural mineral standards. Data were regressed using an oxide-ZAF correction program supplied by JEOL.

A.1. SHRIMP zircon dating

Heavy minerals were separated from whole-rock samples by standard procedures using a jaw crusher, a steel rolling mill and heavy liquids. Zircons were then hand-picked and mounted in epoxy resin together with chips of the standard M257 (Nasdala et al., 2008) for SHRIMP analyses. The mount was ground and polished so that the zircon cores were exposed, and zircons were photographed under cathodoluminescence (CL) to enable an easy and best location on the mount during SHRIMP analyses. CL imaging was done on a 305 Hitachi SEM S-3000N equipped with a Gatan ChromaCL detector and a DigiSan II data306 recorder in the Beijing SHRIMP Center. Operating conditions were 9 kV, 99 μA.

Isotopic analyses were performed on the Beijing SHRIMP II ion microprobe whose instrumental characteristics are identical to that installed in Perth and described by De Laeter and Kennedy (1998). The analytical procedures are outlined in Compston et al. (1992), Claoué-Long et al. (1995), Nelson (1997) and Williams (1998). Prior to each analysis, the surface of the analysis site was cleaned by the rastering of the primary beam for 3 min, to reduce or eliminate surface common Pb. The reduced $^{206}Pb/^{238}U$ ratios were normalized to 0.09101, which is equivalent to the adopted age of 561.3 Ma for standard M257 (Nasdala et al., 2008). Pb/U ratios in the unknown samples were corrected using the ln(Pb/U) / ln(UO/U) relationship as measured in M257 and as outlined in Compston et al. (1992) and Nelson (1997). The 1σ error in the ratio $^{206}Pb/^{238}U$ during analysis of all standard zircons during this study was 1.6%. Primary beam intensity was 9 nA, and a Köhler aperture of 100 μm diameter was used, giving a slightly elliptical spot size of about 30 μm. Peak resolution was 4324 (at 1% peak height) on mass ^{254}OU of the standard, enabling clear separation of the ^{208}Pb-peak from the HfO peak. Analyses of samples and standards were alternated to allow assessment of Pb^+/U^+ discrimination.

Raw data reduction and error assessment followed the method described by Nelson (1997). Common Pb corrections have been applied using the ^{204}Pb-correction method and assuming the isotopic composition of Broken Hill, because common Pb is thought to be surface-related (Kinny, 1986). The analytical data are presented in Table 2. Errors given on individual analyses are based on counting statistics and are at the 1σ level and include the uncertainty of the standard added in quadrature. Errors for pooled analyses are at 2σ. The ages and errors were calculated for mean $^{207}Pb/^{206}Pb$ ratios, including the calibration error on 34 standards measured during the analytical session.

A.2. Nd isotopic analysis

Sm–Nd isotopic analyses were performed at the Institute of Precambrian Geology and Geochronology, RAS, St. Petersburg. About 100 mg of whole-rock powder was dissolved in a mixture of HF, HNO_3 and $HClO_4$. A ^{149}Sm–^{150}Nd spike solution was added to all samples prior to dissolution. REE were separated on BioRad AGW50-X8 200–400 mesh resin using conventional cation-exchange techniques. Sm and Nd were separated by extraction chromatography with a LN-Spec (100–150 mesh) resin. The total laboratory blanks were 0.1–0.2 ng for Sm and 0.1–0.5 ng for Nd. Isotopic compositions of Sm and Nd were determined on a TRITON TI multicollector mass-spectrometer in static mode. The precision (2σ) of Sm and Nd contents and $^{147}Sm/^{144}Nd$ ratios was ca. 0.5% and ca. 0.005% for $^{143}Nd/^{144}Nd$ ratios.

$^{143}Nd/^{144}Nd$ ratios were adjusted relative to a value of 0.511860 for the La Jolla standard. During the period of analysis the weighted average of 9 La Jolla Nd standard runs yielded 0.511852 ± 8 (2σ) for $^{143}Nd/^{144}Nd$, normalized against $^{146}Nd/^{144}Nd = 0.7219$. The $\varepsilon_{Nd(t)}$ values were calculated using the present-day values for a chondritic uniform reservoir (CHUR) $^{143}Nd/^{144}Nd = 0.512638$ and $^{147}Sm/^{144}Nd = 0.1967$ (Jacobsen and Wasserburg, 1984). Whole-rock Nd $t_{Nd(DM)}$ model ages were calculated using the model of Goldstein and Jacobsen (1988) according to which the Nd isotopic composition of the depleted mantle evolved linearly since 4.56 Ga ago and has a present-day value $\varepsilon_{Nd}(0)$ of +10 ($^{143}Nd/^{144}Nd = 0.513151$ and $^{147}Sm/^{144}Nd = 0.21365$). Two-stage or crustal Nd model ages $t_{Nd(c)}$ (Keto and Jacobsen, 1987) were calculated using a mean crustal $^{147}Sm/^{144}Nd$ ratio of 0.12 (Taylor and McLennan, 1985).

A.3. Hf isotopic analysis

Zircon spots previously analyzed on SHRIMP II were selected for Hf isotopic analyses on a Nu Plasma HR MC-ICP-MS (Nu Instruments, UK), coupled to a 193 nm excimer laser ablation system (RESOlution M-50, Resonetics LLC, USA), installed in the Dept. of Earth Sciences, The University of Hong Kong. The instrumental settings are detailed in Xia et al. (2011). Data were acquired by ablating 55 μm (diameter) laser spots, and a 6 Hz repetition rate was used. The analyses consisted of a 30 s blank measurement prior to the start of ablation and 40 s of ablation. The measured isotopic ratios of $^{176}Hf/^{177}Hf$ were normalized to $^{179}Hf/^{177}Hf = 0.7325$, using exponential correction for mass bias. Isobaric interference of ^{176}Yb and ^{176}Lu on ^{176}Hf was corrected by monitoring ^{172}Yb and ^{175}Lu respectively. The in-situ measured $^{173}Yb/^{172}Yb$ ratio was used for mass bias correction for both Yb and Lu because of their similar physicochemical properties. Ratios used for the corrections were 0.5887 for $^{176}Yb/^{172}Yb$ and 0.02655 for $^{176}Lu/^{175}Lu$ (Vervoort et al., 2004). External corrections were applied to all unknowns, and standard zircons 91500 and GJ-1 were used as external standards and were analyzed twice before and after every 10 analyses. The measured $^{176}Lu/^{177}Hf$ ratios and a ^{176}Lu decay constant of 1.865×10^{-11} a^{-1} as reported by Scherer et al. (2001) were used to calculate initial $^{176}Hf/^{177}Hf$ ratios. Calculation of ε_{Hf} values is based on the chondritic values of $^{176}Hf/^{177}Hf$ and $^{176}Lu/^{177}Hf$ as reported by Blichert-Toft and Albarède (1997). The mantle extraction model age $t_{Hf(DM)}$ was calculated using the measured $^{176}Lu/^{177}Hf$ of the zircon, but this only provides a minimum age for the source material of the magma from which the zircon crystallized. Therefore, we also have calculated a crustal model age $t_{Hf(c)}$ (Table 4), which assumes that the parental magma of the zircons was produced from an average lower continental crust ($^{176}Lu/^{177}Hf = 0.010$, Kröner et al., 2013a, 2014) but was ultimately derived from the

depleted mantle. The depleted mantle lines in Fig. 10 are defined by present-day $^{176}Hf/^{177}Hf = 0.28325$ and $^{176}Lu/^{177}Hf = 0.0384$ (Griffin et al., 2004).

References

Afonin, V.P., Finkelstein, A.L., Borkhodoev, V.J., Gunicheva, T.N., 1992. X-ray fluorescence analysis of rocks by the fundamental parameter methods. X-ray Spectrometry 21, 69–75.

Anisimova, I.V., Kozakov, I.K., Yarmolyuk, V.V., Kozlovsky, A.M., Kovach, V.P., Kudryashova, E.A., Savatenkov, V.M., Terent'eva, L.B., Fedoseenko, A.M., Yakovleva, S.Z., Enzhin, G., 2009a. Age, sources, and geological position of anorthosites of Precambrian terranes of Central Asia: example from the Hunzhilingol Massif, central Mongolia. Doklady Earth Sciences 428, 1120–1125.

Anisimova, I.V., Levitsky, I.V., Sal'nikova, E.B., Kotov, A.B., Levitsky, V.I., Reznizkyi, L.Z., Efremov, S.V., Velikoslavinskyi, S.D., Barash, I.G., Fedoseenko, A.M., 2009b. Age of the Gargan Block basement (East Siberia): results of U–Pb geochronological studies. Proceedings of the 4th All-Russia Conference on Isotope Geochronology. Isotope Systems and Timing of Geological Processes. St. Petersburg, Tsentr informatsionnoi kul'tury, 1, pp. 34–35 (in Russian).

Aranovich, L.Ya, Berman, R.G., 1996. Optimized standard state and solution properties of minerals: II. Comparisons, predictions, and applications. Contributions to Mineralogy and Petrology 126, 25–37.

Arndt, N.T., Goldstein, S.L., 1987. Use and abuse of crust-formation ages. Geology 15, 893–895.

Badarch, G., Cunningham, W.D., Windley, B.F., 2002. A new terrane subdivision for Mongolia: implications for the Phanerozoic crustal growth of Central Asia. Journal of Asian Earth Sciences 21, 87–110.

Belousova, E.A., Griffin, W.L., O'Reilly, S.Y., 2006. Zircon crystal morphology, trace element signatures and Hf isotope composition as a tool for petrogenetic modelling: examples from eastern Australian granitoids. Journal of Petrology 47, 329–353.

Berman, R.G., 1991. Thermobarometry using multiequilibrium calculations: a new technique with petrologic applications. Canadian Mineralogist 29, 833–855.

Berman, R.G., Aranovich, L.Ya., 1996. Optimized standard state and solution properties of minerals: I. Model calibration for olivine, orthopyroxene, cordierite, garnet, and ilmenite in the system $FeO–MgO–CaO–Al_2O_3–TiO_2–SiO_2$. Contributions to Mineralogy and Petrology 126, 1–24.

Blichert-Toft, J., Albarède, F., 1997. The Lu–Hf geochemistry of chondrites and the evolution of the mantle–crust system. Earth and Planetary Science Letters 148, 243–258.

Claoué-Long, J.C., Compston, W., Roberts, J., Fanning, C.M., 1995. Two Carboniferous ages: a comparison of SHRIMP zircon dating with conventional zircon ages and $^{40}Ar/^{39}Ar$ analyses. Soc. Sediment. Geol., Spec. Publ., 54, pp. 3–21.

Compston, W., Williams, I.S., Kirschvink, J.L., Zhang, Z., Ma, G., 1992. Zircon U–Pb ages for the Early Cambrian time scale. Journal of the Geological Society of London 149, 171–184.

Corfu, F., Hanchar, J.M., Hoskin, P.W.O., Kinny, P., 2003. Atlas of zircon textures. In: Hanchar, J.M., Hoskin, J.M., P.W.O. (Eds.), Zircon. Reviews in Mineralogy and Geochemistry, Mineralogical Society of America, 53, pp. 468–500.

De Laeter, J.R., Kennedy, A.K., 1998. A double focusing mass spectrometer for geochronology. International Journal of Mass Spectrometry 178, 43–50.

Demoux, A., Kröner, A., Badarch, G., Jian, P., Tomurhuu, D., Wingate, M.T.D., 2009. Zircon ages from the Baydrag Block and the Bayankhongor ophiolite zone: time constraints on late Neoproterozoic to Cambrian subduction- and accretion-related magmatism in Central Mongolia. Journal of Geology 117, 377–397.

DePaolo, D.J., 1988. Neodymium Isotope Geochemistry. Springer Verlag, Berlin (187 pp.).

Dong, C., Wan, Y., Wilde, S.A., Xu, Z., Ma, M., Xie, H., Liu, D., 2014. Earliest Paleoproterozoic supracrustal rocks in the North China Craton recognized from the Daqingshan area of the Khondalite Belt: constraints on craton evolution. Gondwana Research 25, 1535–1553. http://dx.doi.org/10.1016/j.gr.2013.05.021.

Goldstein, S.J., Jacobsen, S.B., 1988. Nd and Sr isotopic systematics of river water suspended material: implications for crustal evolution. Earth and Planetary Science Letters 87, 249–265.

Griffin, W.L., Belousova, E.A., Shee, S.R., Pearson, N.J., O'Reilly, S.Y., 2004. Archean crustal evolution in the northern Yilgarn Craton: U–Pb and Hf-isotope evidence from detrital zircons. Precambrian Research 131, 231–282.

Harris, N.B.W., Bartlett, J.M., Santosh, M., 1996. Neodymium isotope constraints on the tectonic evolution of East Gondwana. Journal of Southeast Asian Earth Sciences 14, 119–125.

Jacobsen, S.B., Wasserburg, G.J., 1984. Sm–Nd evolution of chondrites and a chondrites. II. Earth and Planetary Science Letters 67, 137–150.

Keto, L.S., Jacobsen, S.B., 1987. Nd and Sr isotopic variations of early Paleozoic oceans. Earth and Planetary Science Letters 84, 27–41.

Kinny, P.D., 1986. 3820 Ma zircons from a tonalitic Amitsoq gneiss in the Godthab district of southern West Greenland. Earth and Planetary Science Letters 79, 337–347.

Kovach, V.P., Matukov, D.I., Berezhnaya, N.G., Kotov, A.B., Levitsky, V.I., Barash, I.G., Kozakov, I.K., Levsky, L.K., Sergeev, S.A., 2004. SHRIMP zircon age of the Gargan block tonalites — find early Precambrian basement of the Tuvino-Mongolian microcontinent. Central Asian Mobile Belt. Abstract, 32th International Geological Congress. CD.

Kovalenko, V.I., Kostitsyn, Yu.A., Yarmolyuk, V.V., Budnikov, S.V., Kovach, V.P., Kotov, A.B., Sal'nikova, E.B., Antipin, V.S., 1999. Magma sources and the isotopic (Sr and Nd) evolution of Li–F rare-metal granites. Petrology 7, 383–409.

Kovalenko, V.I., Yarmolyuk, V.V., Tomurtogoo, O., Antipin, V.S., Kovach, V.P., Kotov, A.B., Kudryashova, E.A., Sal'nikova, E.B., Zagornaya, N.Yu., 2005. Geodynamics and crust-forming processes in the early Caledonides of the Bayanhongor zone, central Mongolia. Geotectonics 39, 298–316.

Kozakov, I.K. (Ed.), 1993. Early Precambrian in the Central Asian Fold Belt. Nauka Publishing House, Leningrad (266 pp. (in Russian)).

Kozakov, I.K., Kotov, A.B., Kovach, V.P., Salnikova, E.B., 1997. Crustal growth in the geologic evolution of the Baidarik Block, Central Mongolia: evidence from Sm–Nd isotopic systematics. Petrology 5, 121–207.

Kozakov, I.K., Sal'nikova, E.B., Wang, T., Didenko, A.N., Plotkina Yu, V., Podkovyrov, V. N., 2007. Early Precambrian crystalline complexes of the Central Asian microcontinent: age, sources, tectonic position. Stratigraphy and Geologicalo Correlation 15, 121–140.

Kozakov, I.K., Sal'nikova, E.B., Kovach, V.P., Yarmolyuk, V.V., Anisimova, I.V., Kozlovskii, A.M., Plotkina, Yu.V., Myskova, T.A., Fedoseenko, A.M., Yakovleva, S. Z., Sugorakova, A.M., 2008. Vendian stage in formation of the early Caledonian superterrane in Central Asia. Stratigraphy and Geological Correlation 16, 360–382.

Kozakov, I.K., Kozlovsky, A.M., Yarmolyuk, V.V., Kovach, V.P., Bibikova, E.V., Kirnozova, T.I., Plotkina, Yu.V., Yu, Zagornaya N., Fugzan, M.M., Ch, Erdenejargal, Lebedev, V.I., Eenjin, G., 2011. Crystalline complexes of the Tarbagatai block of the early Caledonian superterrane of Central Asia. Petrology 19, 426–444.

Kretz, R., 1983. Symbols of rock-forming minerals. American Mineralogist 68, 277–279.

Kröner, A., Jaeckel, P., Williams, I.S., 1994. Pb-loss patterns in zircons from a high-grade metamorphic terrain as revealed by different dating methods: U–Pb and Pb–Pb ages for igneous and metamorphic zircons from northern Sri Lanka. Precambrian Research 66, 151–181.

Kröner, A., O'Brien, P.J., Nemchin, A.A., Pidgeon, R.T., 2000. Zircon ages for high pressure granulites from South Bohemia, Czech Republic, and their connection to Carboniferous high temperature processes. Contributions to Mineralogy and Petrology 138, 127–142.

Kröner, A., Rojas-Agramonte, Y., Kehelpannala, K.V.W., Zack, T., Hegner, E., Geng, H.Y., Wong, J., Barth, M., 2013a. Age, Nd–Hf isotopes, and geochemistry of the Vijayan Complex of eastern and southern Sri Lanka: a Grenville-age magmatic arc of unknown derivation. Precambrian Research 234, 288–321.

Kröner, A., Hoffmann, J.E., Xie, H., Wu, F., Münker, C., Hegner, E., Wong, J., Wan, Y., Liu, D., 2013b. Generation of early Archaean felsic greenstone volcanic rocks through crustal melting in the Kaapvaal, craton, southern Africa. Earth and Planetary Science Letters 381, 188–197.

Kröner, A., Kovach, V., Belousova, E., Hegner, E., Armstrong, R., Dolgopolova, A., Seltmann, R., Alexeiev, D.V., Hoffmann, J.E., Wong, J., Sun, M., Cai, K., Wang, T., Tong, Y., Wilde, S.A., Degtyarev, K.E., Rytsk, E., 2014. Reassessment of continental growth during the accretionary history of the Central Asian Orogenic Belt. Gondwana Research 25, 103–125.

Mitrofanov, F.P., Kozakov, I.R., Palei, I.P., 1981. Precambrian of Western Mongolia and Southern Tuva. Nauka Publishing House, Leningrad 155 p. (in Russian).

Mossakovsky, A.A., Ruzhentsev, S.V., Samygin, S.G., Kheraskova, T.N., 1993. Central Asian foldbelt: geodynamic evolution and formation history. Geotektonika 27, 3–33.

Nasdala, L., Hofmeister, W., Norberg, N., Mattinson, J.M., Corfu, F., Dörr, W., Kamo, S.L., Kennedy, A.K., Kronz, A., Reiners, P.W., Frei, D., Kosler, J., Wan, Y., Götze, J., Häger, T., Kröner, A., Valley, J.W., 2008. Zircon M257 — a homogeneous natural reference material for the ion microprobe U–Pb analysis of zircon. Geostandards and Geoanalytical Research 32, 247–265.

Nelson, D.R., 1997. Compilation of SHRIMP U–Pb zircon geochronology data, 1996. Geological Survey of Western Australia, Record 1997/2 (189 pp.).

Panteeva, S.V., Gladkochoub, D.P., Donskaya, T.V., Markova, V.V., Sandimirova, G.P., 2003. Determination of 24 trace elements in felsic rocks by inductively coupled plasma mass spectrometry after lithium metaborate fusion. Spectrochimica Acta Part B: Atomic Spectroscopy 58, 341–350.

Rojas-Agramonte, Y., Kröner, A., Demoux, A., Xia, X., Wang, W., Donskaya, T., Liu, D., Sun, M., 2011. Detrital and xenocrystic zircon ages from Neoproterozoic to Palaeozoic arc terranes of Mongolia: significance for the origin of crustal fragments in the Central Asian Orogenic Belt. Gondwana Research 19, 751–763.

Scherer, E., Münker, C., Mezger, K., 2001. Calibration of the lutetium–hafnium clock. Science 293, 683–687.

Silver, L.T., 1969. A geochronological investigation of the anorthosite complex, Adirondack Mountains, New York. In: Isachsen, Y.W. (Ed.), Origin of Anorthosite and Related Rocks: New York Museum and Science Service, Memoir, 18, pp. 57–82.

Sun, S.-S., McDonough, W.F., 1989. Chemical and isotopic systematics of oceanic basalts: implications for mantle composition and processes. Geological Society of London, Special Publications 42, 313–345.

Taylor, S.R., McLennan, S.M., 1985. The Continental Crust, Its Composition and Evolution. Blackwell, Oxford (312 pp.).

Vervoort, J.D., Patchett, P.J., 1996. Behaviour of hafnium and neodymium isotopes in the crust: constraints from Precambrian crustally derived granites. Geochimica et Cosmochimica Acta 60, 3717–3733.

Vervoort, J.D., Patchett, P.J., Soderlund, U., Baker, M., 2004. Isotopic composition of Yb and the determination of Lu concentrations and Lu/Hf ratios by isotope dilution MC-ICP-MS. Geochemistry, Geophysics, Geosystems 5, Q11002. http://dx.doi.org/10.1029/2004GC000721.

Wan, Y., Liu, D., Dong, C., Xu, Z., Wang, Z., Wilde, S.A., Yang, Y., Liu, Z., Zhou, H., 2009. The Precambrian Khondalite Belt in the Daqingshan area, North China Craton: evidence for multiple metamorphic events in the Palaeoproterozoic era. In: Reddy, S.M., Mazumder, R., Evans, D.A.D., Collins, A.S. (Eds.), Palaeoproterozoic Supercontinents and Global Evolution. Geological Society, London, Special Publications, 323, pp. 73–97.

Wan, Y., Liu, D., Dong, C., Liu, S., Wang, S., Yang, E., 2011. U–Th–Pb behavior of zircons under high-grade metamorphic conditions: a case study of zircon dating of metadiorite near Qixia, eastern Shandong. Geoscience Frontiers 2, 137–146.

Williams, I.S., 1998. U–Th–Pb geochronology by ion microprobe. In: McKibben, M.A., Shanks III, W.C., Ridley, W.I. (Eds.), Applications of Microanalytical Techniques to understanding Mineralizing Processes. Reviews in Economic Geology, 7, pp. 1–35.

Xia, X.P., Sun, M., Geng, H.Y., Wang, Y.J., Zhao, G.C., 2011. Quasi-simultaneous determination of U–Pb and Hf isotope compositions of zircon by excimer laser-ablation multiple-collector ICPMS. Journal of Analytical Atomic Spectrometry 26, 1868–1871.

Yarmolyuk, V.V., Kovach, V.P., Kovalenko, V.I., Salnikova, E.B., Kozlovskii, A.M., Kotov, A.B., Yakovleva, S.Z., Fedoseenko, A.M., 2011. Composition, sources, and growth mechanisms of continental crust in the Lake zone of the Central Asian Caledonides: I. Geological and geochronological data. Petrology 19, 55–78.

Zeh, A., Gerdes, A., Will, T.M., Frimmel, E., 2010. Hafnium isotope homogenization during metamorphic zircon growth in amphibolite-facies rocks: examples from the Shackleton Range (Antarctica). Geochimica et Cosmochimica Acta 74, 4740–4758.

Please cite this article as: Kröner, A., et al., Zircon ages and Nd–Hf isotopes in UHT granulites of the Ider Complex: A cratonic terrane within the Central Asian Orogenic Belt in..., Gondwana Research (2014), http://dx.doi.org/10.1016/j.gr.2014.03.005